Complex Human hear bearing Skin Organoids reveal Cell Type Specific Susceptibility and Innate Immune Responses to Herpes Simplex Virus 1

Emanuel Wyler*[1], Silvia Albertini*[2], Caroline C. Friedel[3], Artür Manukyan[1], Annalena Winterfeldt[4], Nina Bracker[4], Jiabin Huang[4], Susanne Krasemann[5], Izabela Plumbom[6,7], Janine Altmüller[6,7], Thomas Conrad[6,7], Rudolph Reimer[8], Carola Schneider[8], Helena Radbruch[9], Wali Hafezi[10], Arne Hansen[11], Adam Grundhoff[12], Markus Landthaler[1,13], Nicole Fischer[2], Manja Czech-Sioli[4#]

[1] Max Delbrück Center for Molecular Medicine in the Helmholtz Association (MDC), Berlin Institute for Medical Systems Biology, Berlin, Germany
[2] Institute for Molecular Virology and Tumorvirology, University Medical Center Hamburg-Eppendorf Hamburg, Germany
[3] Institute for Informatics, Ludwig-Maximilians-Universität München, Munich, Germany
[4] Institute of Medical Microbiology, Virology and Hygiene, University Medical Center Hamburg-Eppendorf Hamburg, Germany
[5] Institute of Neuropathology, University Medical Center Hamburg-Eppendorf, Hamburg, Germany
[6] Genomics Technology Platform, Max Delbrück Center for Molecular Medicine in the Helmholtz Association, Berlin, Germany
[7] Core Facility Genomics, Berlin Institute of Health at Charité - Universitätsmedizin Berlin, Berlin, Germany
[8] Technology platform Microscopy and Image Analysis/Electron Microscopy, Leibniz Institute of Virology, Hamburg, Germany
[9] Department of Neuropathology, Charité – Universitätsmedizin Berlin, Berlin, Germany
[10] University Hospital Muenster, Institute of Virology / Clinical Virology, Muenster, Germany
[11] Institute of Experimental Pharmacology and Toxicology, University Medical Center Hamburg-Eppendorf, Hamburg, Germany
[12] Department of Viral Genomics, Leibniz Institute of Virology, Hamburg, Germany
[13] Institut für Biologie, Humboldt-Universität zu Berlin, Berlin, Germany

* These authors contributed equally

To whom correspondence should be addressed: m.czech-sioli@uke.de

Abstract

Epithelial surfaces are the initial site of Herpes Simplex Virus 1 (HSV-1) infection. After latency establishment in the peripheral nervous system, reactivation can lead to skin pathologies. To reflect the complexity of skin we used complex human hair bearing skin organoids as a new model system for HSV-1 infection. We analyzed spread of the infection through the three-dimensional tissue and the cell type specific host response in a spatial temporal manner. Single-cell-resolution spatial transcriptomics and imaging shows a restricted viral infection in keratinocytes of the epidermis and hair follicles. The host factor IER3 is upregulated in papillary fibroblasts of the dermis as the infection progresses through the tissue. In keratinocytes of the stratum basale, we find IRF3 upregulated in infected but also virus negative cells, suggesting a signaling mechanism to initiate antiviral responses. Furthermore, we find a cell type specific inflammatory response with an upregulation of TNFSF9 in dermal fibroblasts and TNF in keratinocytes. TNFα target genes are induced in neighboring uninfected cells suggesting the induction of a localized inflammatory reaction to suppress viral infection. In summary, our findings position human hair-bearing skin organoids as a highly physiological model system for studying HSV-1 pathogenesis and reveal spatially organized host responses.

Introduction

Herpes Simplex Virus 1 (HSV-1) is a highly prevalent human pathogen with a global prevalence of ~67% in under 50-year-old individuals[1]. Primary infection usually occurs via the mucosal surfaces or micro-lesions in the skin. Initially HSV-1 productively replicates in the epithelial cells of skin and mucosa causing inflammation and tissue damage and consequently blisters[2]. After replication in epithelial cells, HSV-1 enters the nerve endings of peripheral neurons and travels along their axons to the cell bodies in trigeminal ganglia where it establishes latency[3,4]. Upon spontaneous reactivation, HSV-1 enters the lytic life cycle and produces infectious viral particles that migrate in an anterograde manner to the epithelial cells

63 of skin and mucosa. The following lytic replication in the epithelium leads to the characteristic
64 herpes lesions that release virus to the environment[2].
65 In the past, many different model systems have been used to elucidate the mechanisms of
66 primary infection and reactivation by HSV-1 in the skin. Due to the complexity of skin and the
67 involvement of many different cell types, *in vitro* modelling by monolayer cell cultures can only
68 recapitulate certain aspects of the viral life cycle. More complex model systems used to study
69 virus susceptibility, spread and cytopathic effects are animal models[5-8], *ex vivo* murine[8-10] and
70 human skin explants[8,11,12], and epithelial raft cultures[13,14].
71 While the understanding of HSV-1 pathogenesis in the skin has exceptionally increased using
72 these model systems, many aspects remain elusive. Especially the susceptibility and
73 contributions of specific structures, like hair follicles, different fibroblasts subpopulations and
74 low abundancy cell types, to primary infection, latency establishment and reactivation are not
75 understood. The field of organoids is constantly evolving and creating potential new model
76 systems for virus research[15-17]. In this study we used a highly complex skin organoid (SkO)
77 model generated from human induced pluripotent stem cells (hiPSCs) for the analysis of HSV-
78 1 pathogenesis in the skin[18,19]. SkOs contain a stratified epidermis, fat-rich dermis, hair follicles
79 (HFs) producing pigmented hair, sebaceous glands, melanocytes and Merkel cells. The HFs
80 are innervated by sensory neurons that are covered in Schwann cells on their axons while their
81 somata assemble in trigeminal like clusters together with satellite glial cells. SkOs contain all
82 cell types expected in the fetal skin of the second trimester of development except for sweat
83 glands, vascularization and immune cells[18,19]. Similar to many other organoids, SkOs show an
84 inside out morphology with the dermis being exterior and exposed to the culture medium and
85 the epidermis being interior with hair from hair follicles growing to the inside of the organoid.
86 In this study, SkOs were infected with HSV-1 from the dermal side, leading to viral spread from
87 the dermis to the epidermis, thereby recapitulating primary infection associated with deep
88 dermal wounding or viral reactivation. We analyzed the susceptibility of different cell types to
89 HSV-1 infection and found a restricted HSV-1 infection in keratinocytes as well as in HF cells
90 of both dermal and epidermal origin. Furthermore, we found the host factors IER3 and IRF3

91 upregulated in a spatial temporal manner in response to the infection. We found a spatially
92 restricted inflammatory response by expression of TNF and TNFSF9 leading to downstream
93 activation of TNF target genes. Overall, our study shows how complex infection models
94 combined with high-resolution spatial omics methods allow the investigation of cellular
95 responses and the progression of infection through complex three-dimensional tissues.

96 # Results

97 **Infection of skin organoids (SkOs) with HSV-1**

98 SkOs were produced after the protocol from Lee and collegues[19] and checked for correct
99 differentiation by brightfield microscopy, immunohistochemistry (IHC) and whole-mount
100 immunofluorescence (WMI) staining (Supplementary Figure 1A-D). We observed the expected
101 full complexity at ~120 days of differentiation with the dermis and epidermis in the head
102 structure and cartilage in the tail. The keratinocytes in the epidermis showed a basal layer and
103 differentiation into stratum spinosum and granulosum with terminally differentiated dying
104 keratinocytes accumulating in the head of the SkO (Supplementary Figure 1D). Hair follicles
105 (HFs) showed the expected structures i.e., dermal papilla, matrix, inner root sheath, and outer
106 root sheath. We detected Merkel cells and innervation of the HFs with assembly of neuronal
107 somata in the organoid tail (Supplementary Figure 1B-D).
108 SkOs at 120 days of differentiation were infected with HSV-1 strain 17 expressing GFP under
109 the control of a CMV IE-promoter. To observe spread of the infection within the tissue from
110 single spots, infection was performed with a low viral dose (800 PFU per SkO). At 2dpi GFP
111 expression was visible by fluorescence microscopy at spots on the surface of the organoid
112 (Figure 1A). In IHC staining the first layers of fibroblasts in the dermis showed expression of
113 GFP and HSV-1 glycoprotein D (gD) and indications of a cytopathic effect (CPE). Infection
114 spread solely among cells of the dermis with exclusion of the HFs (Figure 1B, Supplementary
115 Figure 2). At 4dpi GFP fluorescence increased and covered the entire organoid (Figure 1A).
116 IHC staining for GFP and gD showed that the infection reached the inner structures of the
117 organoid including the HFs and keratinocytes of the basal layer and the stratum spinosum.

118 Terminally differentiated keratinocytes showed no signs of infection. Similarly, the different cell
119 layers at the HFs were positive for GFP and gD except for the cornified hair structures (Figure
120 1B, Supplementary Figure 2). Until 8dpi, we observed no sign of infection in these structures,
121 as in the cartilage of the organoid tail. At 4dpi a CPE could be observed mainly in the dermis.
122 At 6dpi infected keratinocytes in the epidermis and the inner cell layers at the HFs started to
123 show a CPE that resulted in dissolvement of the basal membrane and HF integrity. Taken
124 together, these findings showed that HSV-1 infects almost all cell types of SkOs with
125 indications of differential spreading in different cell types.

126 **Bulk transcriptomics of HSV-1 infected skin organoids**

127 To analyze the dynamics of viral gene expression and the host response to the viral infection
128 we performed bulk RNA-seq of uninfected and HSV-1 infected SkOs at 2, 4, 6 and 8dpi. At
129 2dpi we observed only 20 differentially expressed genes (DEGs), which increased to ~1000 at
130 4dpi and ~5000 at 6 and 8dpi (Figure 2A, Supplementary Figure 2B, C). At 4dpi vs. uninfected
131 we found an enrichment of GO-terms of inflammation (e.g., NFκB signaling, response to tumor
132 necrosis factor) in the upregulated differentially expressed genes (Figure 2B). At 6 and 8dpi
133 we found terms of cellular differentiation (e.g., skin development, molting cycle) stand out
134 among the downregulated DEGs. This could reflect the typical HSV-1 induced host cell
135 shutoff[20] and the observed CPE. However, the percentage of viral reads reaches ~20% of all
136 reads already at 4dpi and increases only slightly up to ~25% at 6 and 8dpi (Figure 2C). Overall,
137 this data indicated that key transcriptional changes are to be expected during the first 4 to 6dpi,
138 setting the time frame for subsequent experiments.

139 **Spatial transcriptomics of HSV-1 infected skin organoids**

140 To understand the temporal spatial dynamics of the viral infection and the host response in the
141 SkO model system we performed two spatial transcriptomics experiments with single cell
142 resolution on the Xenium platform. In the pilot experiment, we profiled sections of each 3 SkOs
143 uninfected, at 2dpi, and 6dpi. Due to a strong CPE and HSV-1 induced host cell shutoff, we
144 were not able to perform cell type annotation for most cells at the 6dpi time point (see

145 Supplementary Note for results of the pilot experiment). Therefor, we switched to 2dpi, 3dpi
146 and 4dpi timepoints in the main experiment (Figure 3, Supplementary Figure 3). We quantified
147 the expression of the 470 measured genes, including five viral transcripts (US1, UL27, UL29,
148 UL54 and LAT). Cell type identities were assigned based on cellular transcriptomes (Figure
149 3A-D, Supplementary Figure 3A,C,D, see Supplementary Note for cell type assignment
150 strategy). We identified the expected cell types based on single-cell RNA-sequencing data and
151 immunostainings performed by Lee and colleagues[18,21]. Additionally, we could distinguish
152 between subtypes that coincide with specific localization such as different fibroblast types (e.g.,
153 papillary 1, 2 and mesenchymal) that localize proximal or distal to the epidermis. Keratinocyte
154 subtypes at different stages of differentiation were distinguishable and clearly spatially
155 restricted. We annotated the stratum basale and the stratum corneum while the stratum
156 spinosum and granulosum were combined as one cluster, since the markers in our panel were
157 not sufficient for separation. Cell types of the HFs (dermal sheath, outer root sheath, inner root
158 sheath, matrix, bulge region, dermal papilla) were clearly identified and matched their expected
159 localization. Cell type assignments were also successful in infected SkOs (Figure 3A, D),
160 despite downregulation of host transcripts in infected cells. This can be visualized e.g., with
161 complete loss of PDGFRα mRNA, a pan-fibroblast marker, in highly infected cells due to host
162 cell shutoff[20] (Figure 3B, top panels). However, some highly infected cells, particularly
163 fibroblasts, lost their transcriptional identity and were thus assigned as “undefined” (Figure 3A,
164 gray colored cells, Supplementary Figure 3A). Accordingly, the proportion of “undefined” cells
165 increased in highly infected (4dpi) vs. uninfected organoids but did not exceed ~15% of all cells
166 (Figure 3D).
167 Analysis of the expression of the viral transcripts US1/ICP22, UL54/ICP27, UL29/ICP8,
168 UL27/gB and LAT matched the protein staining, showing infection starting in the outermost
169 fibroblast layers of the dermis at 2dpi and then spread through the organoid until the infection
170 reached the epidermis at 4dpi (Figure 3C and Supplementary Figure 3B).

171 **Susceptibility to viral infection varies widely between cell types**

172 To investigate susceptibility and viral gene expression between different cell types in SkOs,
173 we considered the special features of an infection spreading in a tissue compared to an
174 infection in a monolayer cell culture. HSV-1 infects the outer layers of the organoids first and
175 later the more inner parts leading to an asynchronous infection. First, we calculated the
176 proportion of infected cells and the viral load in the most abundant subtypes, papillary
177 fibroblasts type 1/2, keratinocytes of the stratum basale and stratum spinosum/granulosum,
178 and four cell types in HFs (dermal sheath, dermal papilla, outer root sheath, inner root sheath;
179 Figure 4A). At 3dpi papillary fibroblasts type 1, which is the outermost cell layer of SkOs, and
180 the dermal sheath fibroblasts had the highest number of HSV-1 infected cells (~25%). Also,
181 papillary fibroblasts type 1 had a significantly higher viral load than all other cell types including
182 the dermal sheath. At 4dpi, when the infection reaches the inner parts of the organoid, the
183 proportion of infected cells increased in all cell types. However, stratum basale and
184 spinosum/granulosum keratinocytes still showed significantly less infected cells than papillary
185 fibroblasts (Figure 4A, upper panel). Viral loads were significantly lower than in papillary
186 fibroblasts type 1 in all cell types except papillary fibroblasts type 2 (Figure 4A, lower panel).
187 To exclude that this effect was caused by the asynchronous infection spreading from the
188 outside to the inside we compared stratum basale keratinocytes with papillary fibroblasts at
189 equal distance ranges from the exterior surface (Supplementary Figure 4AB). Again, we found
190 significantly lower viral loads. Furthermore, we analyzed the influence of infectious cells in
191 proximity to basal keratinocytes (<50µm distance) (Supplementary Figure 5A). Infectious cells
192 were defined as cells with 20% or more viral transcripts. As expected, we found an increase
193 of the viral load with rising numbers of infectious cells in the neighborhood. Interestingly,
194 papillary fibroblasts reached their maximum viral load (up to 70% viral transcripts) with 1 to 2
195 infectious cells in proximity. Keratinocytes of the stratum basale showed a significantly lower
196 viral load compared to papillary fibroblasts despite the same number of infectious cells in their
197 neighborhood. Even with >6 infectious cells in proximity the mean viral load did not exceed
198 25% of all transcripts. To analyze the dynamics of the viral life cycle we ordered and binned

199 infected cells along increasing viral load. We found in papillary fibroblasts a strong increase of
200 UL54 RNA at the beginning followed by a plateau, with the LAT RNA constantly accumulating
201 (Figure 4B, top panel). In stratum basale keratinocytes, there was an indication of a longer lag
202 phase, and a slower increase of viral gene expression (Figure 4B, bottom panel). These results
203 suggest that keratinocytes of the stratum basale have a delayed or restricted viral life cycle.
204 In dermal sheath fibroblasts, the dermal papilla and the keratinocyte subtypes of HFs (e.g.,
205 matrix, root sheaths) we also observed significantly lower viral loads than in the surrounding
206 papillary fibroblasts (Figure 4A). Staining for the viral early protein ICP8 and the late protein
207 gC showed that viral infection spreads first into the dermis and excludes the HF layers (Figure
208 4C). HF cell layers are infected after the infection already spread to the inner parts of the
209 organoids at 4dpi with the dermal papilla being infected last (Figure 4C, right panel) but
210 eventually infection reaches all layers of HFs with a CPE being observable at 6 to 8dpi (Figure
211 1B). We hypothesized three potential explanations for this observation. First, there could be a
212 layer of non-permissive cells surrounding the HFs. Second, a barrier of extracellular matrix
213 might act protectively. And third, the infection cycle in the different cell types within the HFs
214 could be slower compared to e.g., the surrounding papillary fibroblasts. To investigate these
215 possibilities, we defined dermal sheath fibroblasts located next to highly infected papillary
216 fibroblasts (Supplementary Figure 5B). Indeed, the viral load in these dermal sheath fibroblasts
217 showed a strong drop from the cells outside in direct proximity (Figure 4E). As for keratinocytes
218 of the stratum basale, the lower viral load in cell types of HFs was not driven by spatial effects
219 like the localization relative to the organoid boundary or a lower number of infected cells in
220 proximity (Supplementary Figure 4AB, Supplementary Figure 5A). IF staining of the analyzed
221 cells showed close contact between dermal sheath and papillary fibroblasts with no indication
222 of any physical barriers between these cell layers (Supplementary Figure 5C). This is
223 supported by electron microscopy which showed close proximity of papillary fibroblasts and
224 dermal sheath fibroblasts (Figure 4F, Supplementary Figure 6). We observed that at 3dpi many
225 viral particles are present in the papillary fibroblasts layer inside cells (nucleus/cytoplasm) as
226 well as in the extracellular space (Figure 4F, zoom-ins). In the dermal sheath layer, the matrix,

227 the outer, and inner root sheath we found only a small number of viral particles in the cytoplasm
228 and the nucleus but not in the extracellular space. In the nuclei we found viral A and C capsids
229 indicating viral replication (A-capsids lack DNA, B capsids lack DNA but contain the scaffolding
230 protein and C-capsids contain the viral DNA[22]) (Figure 4F, 3dpi, zoom-in on matrix). In the
231 inner layers of the HF we did not find any viral particles. However, at 4dpi we find viral particles
232 in the extracellular space, the cytoplasm, and the nucleus in almost all HF layers present in
233 our sections (dermal sheath, outer root sheath, matrix, inner root sheath cuticle, companion
234 layer, Huxley's layer, dermal papilla) except for the Henle's layer (Figure 4F, Supplementary
235 Figure 6B). Again, we found A- and C- but also B-capsids in replication compartments of the
236 nucleus in these HF cell types. From these results we conclude that HSV-1 lytically replicates
237 in most cell types of HFs but similar to keratinocytes of the stratum basale viral replication is
238 delayed in these cells which slows down viral spread.

239 **IER3 is induced at the infection front**

240 HSV-1 infection leads to a general shutoff of host genome transcription [20] as well as read-
241 through [23] and antisense transcription [24], but also induction of several genes [25-28]. We used the
242 spatial transcriptomics data to investigate how host gene expression changes are related to
243 the spread of the virus through the tissue. First, we focused on papillary fibroblasts, the most
244 abundant infected cell type. We subclustered cells based on a set of 190 genes deregulated
245 upon infection in papillary fibroblasts (Figure 5AB). By projecting the clusters back onto the
246 section of a 3dpi organoid shown in Figure 3, we observed that the transcriptome-based
247 clustering is reflected in space (Figure 5C). On the one hand, this allowed us to estimate the
248 initial infection site from which the virus gradually spread through the tissue. On the other hand,
249 we could use the gene expression data to investigate what happens at, before and after the
250 "infection front" in a spatial-temporal manner. We calculated DEGs between sets of papillary
251 fibroblasts at different locations (Supplementary Figure 7A-C) which showed that the host gene
252 IER3 is strongly induced at the infection front, with subsequently decreasing in cells later in the
253 viral life cycle (Figure 5C). This is consistent with the transient changes observed in bulk RNA-
254 seq (Supplementary Figure 7D). IER3 is a target gene of the MAP kinase pathway[29] and HSV-

255 1 infection has been shown to stabilize IER3 through ICP27 via this pathway[30-32]. To
256 corroborate our finding, we performed IER3/ICP8 co-immunostaining in whole-mount
257 organoids (Figure 5D). Also, the IER3 protein appears immediately upon infection, but in
258 contrast to the mRNA, it was also upregulated in cells after the infection front that are later in
259 the viral life cycle. Overall, this example shows how genes can be transiently upregulated at
260 the infection front as infection progresses through the tissue, thus creating a specific virus-host
261 cell interaction microenvironment.

262 **HSV-1 infection upregulates the transcription factor IRF3 in keratinocytes**

263 Since defining an "infection front" requires a high number of infected cells from a specific cell
264 type, we could not perform this approach with the lower abundant cell types in our model
265 system. To identify here host genes responding to the infection, we calculated differential
266 expression values per cell type between infected and uninfected organoids. To take the viral
267 RNA content into account, we separated cells into (i) no viral RNA (less than 2 HSV-1 counts),
268 (ii) low virus RNA (viral load below the median calculated within the cell type and time point
269 but across all individual organoids) and (iii) high virus RNA (viral load above the median)
270 (Figure 6A). As positive controls, DUX4, antisense and read-through transcripts were all found
271 to be induced by HSV-1 infection, although to different extent in different cell types.
272 (Supplementary Figure 8A).
273 For further analysis, we focused on genes involved in interferon signaling and present in the
274 gene panel, namely the transcription factors interferon regulatory factor 3 and 9 (IRF3/IRF9),
275 as well as the antiviral, interferon-stimulated gene (ISG) MX Dynamin Like GTPase 1 (MX1)[33].
276 For MX1, we did not find a strong upregulation (Figure 6A). This is in line with the observation
277 that the interferons (IFNs) α, β and γ included in our panel showed no upregulation. Also in
278 bulk RNA-seq we did not find upregulation of interferons at any timepoint. For IRF9 and
279 particularly IRF3 however, we observed clear indications of upregulation in keratinocytes early
280 on, including cells not containing any viral RNA (Figure 6A). Interestingly, this effect was not
281 detectable in bulk RNA-seq (Supplementary Figure 8B). As a confirmation, we found an
282 upregulation of IRF3 also on the protein level, but only when keratinocytes were virus positive

283 (Figure 6B). This suggests a delay of the IRF3 response on protein level, similar to our
284 observation with IER3.

285 **HSV-1 induces a spatially coordinated expression of TNF family cytokines**

286 In our bulk RNA-seq experiment we found that genes involved in response to TNF were
287 overrepresented in the significantly upregulated genes at 4dpi (Figure 2B). The cytokines TNF
288 (coding for TNFα) and TNFSF9 (coding for 4-1BBL) were significantly upregulated by HSV-1
289 infection in bulk- RNA-seq (Supplementary Figure 8B). Notably, spatial transcriptomics
290 showed, that their expression is highly cell type-dependent and largely mutually exclusive, with
291 TNF induced in keratinocytes (mainly stratum basale) and TNFSF9 in papillary fibroblasts with
292 expression of both cytokines clearly depending on viral presence (Figure 7A). Their expression
293 increased with increasing viral load up to a plateau level (Figure 7B). Published data from HSV-
294 1 infected fibroblasts[23] and HaCat keratinocytes[34] support the findings of a cell type specific
295 upregulation of TNFSF9 in fibroblasts and TNF in keratinocytes. Importantly, both the bulk
296 RNA-seq data generated here in SkOs as well as the published bulk RNA-seq did not indicate
297 that upregulation of TNF and TNFSF9 are results of HSV-1 induced read-in transcription from
298 an upstream gene. To investigate, whether expression of TNF would lead to functional sensing
299 in surrounding cells, we defined papillary fibroblasts proximal to TNF expressing cells
300 (Supplementary Figure 8C) and analyzed them for induction of TNFα target genes (Figure 7D)
301 based on a published RNA-seq data set generated in fibroblasts[35]. By calculating the
302 differential expression in cells proximal vs. distal to the TNF-expressing cells we found that
303 four of the 8 genes included in our panel were significantly upregulated especially in cells
304 without viral gene expression (Figure 7D). By focusing on CXCL2, a TNFα-induced gene, we
305 found a high number of cells expressing CXCL2 in the dermis close to TNF expressing
306 keratinocytes (Figure 7C, upper row, last panel). To investigate whether this could also be
307 caused by 4-1BBL (TNFSF9), we analyzed a region with high TNFSF9 but low TNF expression
308 (Figure 7C, lower row). CXCL2 levels in these regions were lower, suggesting that the cell-
309 type specific induction of the TNF gene leads to secretion of the TNFα cytokine and
310 subsequently induction of target genes in the immediately surrounding cells.

311 ## Discussion

312 In this study, we showed an infection of complex human hair bearing skin organoids with HSV-
313 1. Due to the inside-out morphology of the organoids and the infection therefore starting from
314 the dermis our model is closest to the reactivation scenario of HSV-1, when infectious particles
315 are released from neuronal cells into the fibroblast layer of the dermis[36]. This makes our model
316 highly relevant for investigating HSV-1 induced pathologies, since most of them are a result of
317 reactivation and not primary infection. For instance, recurrent herpes labialis has an average
318 incidence of about 1.6 per 1000 patients each year[37].
319 When analyzing the susceptibility of the cells to HSV-1 in the SkO model we found that
320 eventually at 8dpi all cell types in our model system were infected by HSV-1 except for the
321 terminally differentiated keratinocytes, cornified structures in the HFs and chondrocytes in the
322 tail. This is expected due to a lack of immune cells that could clear the infection. At the moment,
323 we do not understand why chondrocytes are resistant to viral infection. A resistance of the
324 stratum corneum against HSV-1 infection has been reported by many other studies using
325 mouse models and *ex vivo* skin showing that the cornified keratinocyte layer prevents HSV-1
326 infection by the external surface[6,9]. The terminally differentiated keratinocytes of the epidermis
327 in the skin organoid model express markers of the stratum corneum (LOR, KRT10), however,
328 they do not eventually cornify since they are not exposed to air. Despite this difference their
329 complete resistance to infection is well in line with findings from other models. Studies also
330 showed that infection of all other layers of the epidermis by HSV-1 strongly depends on the
331 infection route and the model system (dermal vs. epidermal, human vs. mouse, skin vs.
332 mucosal skin)[38,39]. In human *ex vivo* skin wounding from the external side through different
333 approaches leads to only limited infection of the epidermis[11,12]. Only infection from the dermal
334 side by either removal of the dermis or deeper wounding through the epidermis into the dermis
335 leads to efficient infection of the basal keratinocytes and spread to the higher differentiated
336 keratinocyte layers[9,40]. In the SkO model the dermis was efficiently infected by HSV-1 and viral
337 loads in papillary fibroblasts were much higher than in keratinocytes of the stratum basale and
338 stratum spinosum/granulosum despite the presence of infectious cells in the neighborhood.

339 While the basal membrane as an extracellular matrix barrier likely slows down viral infection,
340 we show evidence that the viral life cycle in keratinocytes is delayed compared to papillary
341 fibroblasts. When we analyzed the spread of HSV-1 into HFs we observed that dermal sheath
342 fibroblasts pose a barrier to HSV-1 infection of the more inner layers. The close physical
343 proximity of dermal sheath fibroblasts to heavily infected papillary fibroblasts, in the absence
344 of an intervening or expanded extracellular matrix, suggests that extracellular matrix structures
345 are unlikely to account for the observed barrier function. Furthermore, the finding that dermal
346 sheath cells are not infected less frequently but instead harbor a reduced viral load indicates
347 that this phenotype is unlikely due to limited accessibility of a viral entry receptor, but rather
348 reflects a delayed viral life cycle in this cell type. Our electron microscopy impressively shows
349 that eventually almost all cell types in the HFs produce mature viral particles that were found
350 intra- and extracellular. We hypothesize that the delayed HSV-1 infection in HFs could be
351 important during reactivation when viral particles are released by the nerve endings of sensory
352 neurons that innervate HFs. A restriction of the viral life cycle in dermal sheath fibroblasts could
353 give immune cells time to counteract the infection. In the future, we would like to test this
354 hypothesis by further analyzing the immune reaction in dermal fibroblasts and by including
355 immune cells into the SkO model.
356 Also, we could show that the host response to HSV-1 infection in the SkO model is very cell
357 type specific. We analyzed this on single cell level, but also in a spatial-temporal manner by
358 analyzing cells at the infection front in the dermis. We found IER3 transcripts specifically
359 upregulated in papillary fibroblasts at the leading edge of the infection. IER3 mRNA contains
360 an AU-rich instability element (ARE) in its 3'UTR, a feature that promotes rapid mRNA
361 degradation by deadenylation under normal conditions and stabilization by proinflammatory
362 signaling like the p38 MAPK pathway[41,42]. Many studies have shown before in cell culture that
363 the IER3 mRNA is stabilized by HSV-1[30,31], in particular by ICP27[32]. Interestingly, transcript
364 upregulation was transient, while the upregulated protein was very stable in the heavily
365 infected cells in SkOs. A study using HeLa cells showed a transient induction of IER3 protein

366 expression at 1 hour post infection (hpi) and a rapid decline already at 3hpi[31]. This could
367 indicate a different turnover of the IER3 protein in tissue in comparison to a cell line.
368 The fact that we found a well known target of HSV-1 infection by our spatial temporal analysis
369 shows the validity of the approach. It allows a comprehensive analysis of spatial
370 transcriptomics data from infected tissues that goes beyond the discrimination between cell
371 types and viral loads. However, IER3 was one of only three genes specifically upregulated at
372 the infection front. This is likely an effect of the limited number of host genes included in our
373 spatial transcriptomics experiment (470 genes) and we speculate that panels with more genes
374 included will be even more informative to understand how a tissue reacts to a locally spreading
375 infection. Another limitation of this approach is that for defining an infection front a certain
376 number of cells from a specific cell type is needed, so we could perform this only for papillary
377 fibroblasts of the dermis. Thus for lower abundant and spatially more distributed cells we
378 compared uninfected cells and cells with low viral load and high viral load assuming that cells
379 with a higher viral load have been infected for a longer time. We found that IRF3 is upregulated
380 at transcript and protein level in keratinocytes of the stratum basale. Similar to IER3 we find a
381 delayed effect of protein induction in comparison to the transcripts and no induction of IRF3 on
382 protein level in virus negative cells. Since we do not find induction of IFNα, β or γ, or the ISGs
383 included in our panel we can only speculate which downstream signaling might be induced by
384 IRF3. An indication for a potential antiviral effect is that IRF3 protein is mainly upregulated in
385 infected keratinocytes of the stratum basale where we also found lower viral loads in
386 comparison to fibroblasts of the dermis.
387 The host response to HSV-1 infection in SkO is further dominated by inflammation. Spatial
388 transcriptomics showed that TNF (coding for TNFα) was induced in keratinocytes of the
389 stratum basale, and TNFSF9 (coding for 4-1BBL) in papillary fibroblasts. We also observed
390 induction of TNF target genes in surrounding cells and a potential priming of adjacent
391 uninfected cells, indicating that gene activation is indeed functional. Induction of TNF and
392 subsequent tissue damage was previously associated with HSV-1 in cerebral infections[43]. In
393 *ex vivo* mouse whole corneal culture HSV-1 spread was reduced by TNF treatment but also

394 resulted in increased cell death[44]. In skin it is likely that the strong inflammatory reaction
395 induced by the different TNF cytokines helps to limit viral replication in the case of reactivation
396 in a cell type specific manner. The drawback is the induced tissue damage, but it also offers
397 opportunities to specifically reduce HSV-1 induced inflammation and tissue damage by
398 treatment with inhibitors for TNF or TNFSF9.
399 In summary, we show here that SkOs are a physiologically highly relevant model system for
400 HSV-1 infection in the skin. The combination with single-cell-resolution spatial transcriptomics
401 enabled an unprecedented detailed analysis of viral gene expression and host response.
402 Compared with *ex vivo* skin models, SkOs offer key advantages, including the feasibility of
403 genetic manipulation and prolonged maintenance in culture. These features make SkOs
404 particularly well suited for investigating HSV mutants with growth defects, for studies of viral
405 persistence and latency as well as drug testing. The limitations of the SkO model system lie in
406 the lack of immune cells and vascularization, but a recent study reported the successful
407 incorporation macrophages and improved angiogenesis in SkOs[21]. Building on these
408 advances, future work will aim to further refine this model for HSV-1 and deepen our
409 understanding of HSV-1 pathogenesis in the skin.
410

411 ## Material and Methods

412 **Skin organoid generation**

413 Skin organoids (SkOs) were generated from the human iPS cell line UKEi001-A
414 (RRID:CVCL_A8PR). All procedures involving hiPSC lines were approved by the local ethics
415 committee in Hamburg (Az PV4798, 28.10.2014). HiPSCs were cultivated in six-well plates
416 coated with Geltrex (Thermo Fisher Scientific, cat. no. A1413302) in StemFlex medium (Gibco,
417 cat. no. A3349401) under standard conditions (37°C, 5% CO_2). Generation of SkOs was
418 performed according to the protocol by Lee and colleagues[19] with hiPSCs between passages
419 31-39. Only SkOs showing correct differentiation as determined by the appearance of HFs
420 (HF) at 110 to 120 days post differentiation were used for further experiments.

421

422 **Virus infection**

423 HSV-1 17 CMV-IEproEGFP expressing EGFP under the control of the CMV IE promoter was
424 described before[45]. The virus was propagated on Vero cells and the infection titer determined
425 by plaque assay. Medium on SkOs was exchanged and infection was performed by adding
426 800 PFU per SkO to the medium. After 12hrs the medium was exchanged with standard SkO
427 growth medium and afterwards complete medium exchange was performed every day.

428

429 **Immunostaining and microscopy**

430 For immunohistochemistry SkOs were fixed in 4% phosphate buffered formalin over night at
431 4°C and then transferred to PBS. Afterwards they were protected in 3% agarose, dehydrated
432 using a Leica ASP300S tissue processor, and embedded in paraffin. Organoid paraffin
433 sections were cut at 3 µm and stained with hematoxylin and eosin (H&E) according to standard
434 procedures. For immunohistochemical staining the sections were processed as following: After
435 dewaxing and inactivation of endogenous peroxidases (3% hydrogen peroxide), antibody
436 specific antigen retrieval was performed using the Ventana BenchMark XT autostainer
437 (Ventana, Tuscon, Arizona, USA). Sections were blocked and afterwards incubated with the
438 primary antibodies, see Table S1. For detection of specific binding and DAB staining, the
439 UltraView Universal DAB Detection Kit (Roche, #760-500) was used, which contains both, anti-
440 mouse and anti-rabbit secondary antibody. Counter staining and bluing were performed with
441 Hematoxylin (Ventana Roche, # 760-2021) and Bluing Reagent (Ventana Roche, # 760-2037)
442 for 4 min. Subsequently, stained sections were mounted in mounting medium.
443 Pictures of IHC staining were acquired with the Sysmex Pannoramic MIDI II slide scanner.
444 Image cropping was performed with QuPath0.4.3 and pictures assembled with Adobe
445 Illustrator.
446 For whole mount staining of SkOs the qCe3D method was used according to Lee and
447 colleagues[19] with the following adjustments: Clearing was performed for 48hrs and stained and
448 cleared SkOs were mounted in iSpacer (SUNJinLab) 4 well imaging spacers. For antibodies

449 see Supplementary Table S1. Imaging was performed with a Leica TCS SP8 X confocal
450 microscope. Images were processed with Imaris and ImageJ 2.14 and pictures assembled
451 with Adobe Illustrator.
452

453 **Electron microscopy**

454 SkOs were fixed overnight in 2% paraformaldehyde and 2.5% glutaraldehyde, washed in PBS,
455 and post-fixed in 1% osmium tetroxide for 60 min. Following additional rinses in PBS and
456 double-distilled water, samples were stained with 1% aqueous uranyl acetate for 60 min,
457 dehydrated through a graded ethanol series, and embedded in Epon (Carl Roth). Ultrathin
458 sections (50 nm) were prepared using an Ultracut microtome (Leica Microsystems) and post-
459 stained with 1% uranyl acetate in ethanol. Transmission electron micrographs were acquired
460 on a FEI Tecnai G20 Twin operated at 80 kV and equipped with a 2K CCD Veleta camera
461 (Olympus SIS). For correlating TEM data across entire organoids, serial sections were
462 mounted on silicon wafers and imaged using a Tescan Clara SEM with backscattered-electron
463 detection at 2.8 kV.

464 **Bulk RNA-seq**

465 For bulk RNA-sequencing 4 SkOs per condition (uninfected, 2 days post infection (dpi), 4dpi,
466 6dpi, 8dpi) were used. Total RNA was isolated individually from each SkO by adding QIAzol
467 lysis reagent (Qiagen) and disrupting the organoid by grinding with a pestle. The lysate was
468 homogenized with a QIAshredder (Qiagen). After one round of chloroform extraction, RNA was
469 cleaned up with the RNeasy MinElute Cleanup Kit (Qiagen). DNA was two times digested with
470 the DNA-free DNA removal kit (Thermo Fisher Scientific). RNA concentration was determined
471 with the Qubit RNA broad range assay (Thermo Fisher Scientific) and equal amounts of RNA
472 from two SkOs of the same condition were pooled resulting in duplicates for each condition for
473 sequencing. RNA integrity was determined via a Bioanalyzer RNA 6000 Pico Assay (Agilent,
474 5067-1514). RIN values were in the range between 5.5 and 9.2. From each pooled sample
475 520 ng total RNA was subjected to rRNA depletion (following the Lexogen RiboCop rRNA
476 Depletion Kit for Human/Mouse/Rat V2 protocol, catalog number: 144.24) and further

477 processed via the RNA-Seq V2 Library Prep Kit with UDIs (Lexogen, catalog number: 175.96)
478 in the short insert size variant (RTM) according to manufacturer's instructions. Libraries were
479 quality controlled on a Bioanalyzer High Sensitivity DNA Assay (Agilent, 5067-4626) and were
480 sequenced on an Illumina NextSeq 500 instrument with NextSeq 500/550 High Output Kit v2.5
481 (75 Cycles, product number: 20024906) in a single-read mode (1 x 83 bp). After demultiplexing
482 via bcl2fastq, 20.7 – 28.6 million (M) read pairs assigned to each sample. All samples passed
483 quality control by fastqc and were subjected to downstream analysis. Processing was done
484 with the nf-core/RNA-seq pipeline (v3.12.0) within the nf-core framework[46]. The pipeline was
485 executed with Nextflow v23.04.1[47], utilizing STAR (v2.6.1d)[48] for alignment to the GRCh38
486 human genome and Human herpesvirus 1 genome (X14112.1), as well as Salmon (v1.10.1)[49]
487 for transcript-level quantification based on STAR's alignment output. To eliminate duplicate
488 reads, the --with_umi option was enabled. Gene-level quantification was derived from
489 transcript-level estimates using the R package tximport (v1.34.0)[50], which sums transcript
490 abundances for each gene. The generated raw gene-level counts were normalized and
491 variance-stabilized using the regularized log transformation (rlog) from DESeq2 (v1.34.0)[51],
492 addressing the variance-over-mean trend. Principal component analysis (PCA) confirmed high
493 reproducibility across biological replicates. Differential expression analysis was performed
494 using DESeq2, identifying genes as significantly differentially expressed (DEGs) if they
495 exhibited a fold change ≥ 2 and an adjusted P-value ≤ 0.05. The normalized rlog-transformed
496 counts were then used for clustering and visualization. An overrepresentation analysis of
497 differentially expressed host genes (padj. ≤0.05 and log2FC ≥1/≤-1) was performed with
498 WebGestalt[52]. GO terms associated with "Biological processes noRedundant" were selected
499 with an FDR ≤0.01.

500 **Spatial transcriptomics experiments**

501 SkOs were imbedded in paraffin as described for IHC staining. 3 SkOs for each condition were
502 assembled in one agarose mold before embedding all conditions (uninfected/2dpi/3dpi/4dpi
503 for the main experiment, uninfected/2dpi/6dpi for the pilot experiment). *In situ* RNA
504 measurements were performed using the Xenium system (10x Genomics). The pilot

505 experiment was done at the MDC/BIH genomics platform using nuclear expansion based on
506 DAPI staining for cell segmentation. The main experiment was performed at the 10xGenomics
507 facility in Stockholm using multimodal segmentation (nuclear stain, RNA and protein-based
508 cell staining, cell surface staining). For both experiments, the human multi tissue gene panel
509 was used, supplemented by the 100 genes custom panel CZBXK3 (Supplementary Table 1).
510 Sections of 5µm thickness were placed on a Xenium slide according to the manufacturer's
511 protocol, with drying at 42°C for 3 hours and overnight placement in a desiccator at room
512 temperature, followed by deparaffinization and permeabilization to make the mRNA
513 accessible. The Probe Hybridization Mix was prepared according to the user guide
514 (CG000582, Rev D, 10x Genomics). The staining for Xenium was performed using Xenium
515 Nuclei Staining Buffer (10x Genomics product number: 2000762) as a part of the Xenium
516 Slides & Sample Prep Reagents Kit (PN-1000460). Following the Xenium run, Hematoxylin
517 and Eosin (H&E) staining was performed on the same section according to the Post-Xenium
518 Analyzer H&E Staining user guide (CG000613, Rev B, 10x Genomics).

519 **Spatial transcriptomics analysis**

520 The spatial transcriptomics data was analyzed in R using the VoltRon package[53], as well as
521 packages from tidyverse[54]. Other packages used include DESeq2[51], apeglm[55], sf[56] and
522 concaveman[57]. Briefly, we first assessed cell type identity only on cellular transcriptomes, i.e.
523 without taking spatial information into account (Supplementary Table 2 and see Supplementary
524 Note for more information). Viral load was defined as percent viral counts (i.e., sum of the five
525 viral genes UL54, US1, UL27, UL29, LAT) of all counts per cells. Cells with 10 or less cellular
526 RNA counts were filtered out. Organoid boundaries and distances from these boundaries were
527 identified using the concaveman/st_boundary/st_distance function from the concaveman[57] and
528 sf[56] R packages. To classify cells based on the number of infectious cells in the neighborhood,
529 the absolute number of cells with more than 20% viral load and within 50µm (centroid to
530 centroid distance) was counted for every cell. Differential expression using DESeq2[51] was
531 calculated as pseudo-bulk per cell type, i.e., counts were summed up per group (uninfected
532 and 2dpi all cells, 3 and 4dpi either cells with 1 or less viral count “-” , viral load below “+” , or

533 above the median "++" within the group). The infection front analysis was initiated by clustering
534 papillary fibroblasts with at least 2 viral counts using only genes that are differentially
535 expressed upon infection. Cells of cluster 1, with the lowest viral load, which were in groups of
536 at least 5 cells within 150 micrometers, were defined as the infection front. Cells with less than
537 2 viral counts and within 50µm of these cells were classified as "uninfected next to infection
538 front". For the TNF proximity analysis, cells were defined as "TNF expressing", if at least 3 cells
539 with at least 1 TNF gene count were not more than 30 µm apart from each other, and the
540 proximal area defined at 280 µm around these cells. ChatGPT (OpenAI,
541 https://chat.openai.com, model 5) assisted in writing R code.
542
543 **Data and code availability**
544 Bulk RNA-seq data were deposited at NCBI under BioProject accession number
545 PRJNA1378132, and the raw sequencing reads are available in the NCBI Sequence Read
546 Archive (SRA) under accession numbers SRR36379728–SRR36379737. Spatial
547 transcriptomics data are available through NCBI GEO (accession number GSE313919).
548 Code for spatial transcriptomics and bulk RNA-seq data analysis is available at
549 https://github.com/LandthalerLab/SkinOrganoids_HerpesSimplexVirus1.
550

551 ## Acknowledgements

552 The authors thank Robert Shelansky, Aishwarya Konnur, Jana Lalakova, Morgane Rouault
553 (10xGenomics) for performing the main spatial experiment in this manuscript and for technical
554 support. Vera Wolf, Kathrein Permien (Charité) and Kristin Hartmann (Core Facility
555 Experimental Histo-Pathology/UKE) provided technical assistance. We thank the UKE imaging
556 facility (umif) for technical support in microscopy. We thank Claudia Schmidt, Lisann Röpke,
557 Josephine Bonath and Oula Moshilam (UKE) for technical assistance in iPSCs and organoid
558 culture. We thank Patrick Blümke (Technology Platform Next Generation Sequencing, LIV) for
559 technical support in bulk RNA-seq.

This work was supported by the Deutsche Forschungsgemeinschaft (DFG; German Research Foundation) in the framework of the Research Unit FOR5200 DEEP-DV (443644894) project, CZ 320/1-1, GR 3318/5-1, LA 2941/18-1, FR 2938/11-1 and FI 782/7-1 to M.C.-S., A.G., M.L., C.C.F. and N.F., respectively. M.C.-S. was supported by PIER (Partnership of Universität Hamburg and DESY) project PIF-2023-13.

Contributions

Conceptualization: E.W., S.A., A.G., M.L., N.F., M.C.-S

Methodology:. E.W., S.A., A.W.,M.C.-S.

Investigation: E.W.,S.A., A.W., N.B., S.K., R.R., C.S., H.R., M.C.-S.

Data analysis: E.W., C.C.F., J.H., M.C.-S.

Resources (reagents and techniques): E.W., A.M., I.P., J.A., T.C., W.H., A.H., A.G., M.L., N.F, M.C.-S.

Writing – original draft: E.W., M.C.-S.

Funding acquisition: A.G., C.C.F., M.L., N.F., M.C.-S.

All authors discussed the results, contributed to manuscript editing, and approved the final version.

Competing interests

The authors declare no competing interests.

Figure legends

Figure 1: Infection of skin organoids with HSV-1 leads to cytopathic effects. A: Brightfield (BF) and fluorescence (GFP) images of skin organoids (SkOs) infected with HSV-1 (expressing GFP from a CMV-IE promoter) at 120 days of differentiation. Shown are uninfected and HSV-1 infected SkOs at 2, 4, 6, and 8 days post infection (dpi). Scale bars 500µm. **B:** IHC staining of SkOs infected with HSV-1 as shown in A. Boxes in overview images indicate areas

587 of higher magnification shown below. Scale bars 500µm in overview images and 20µm in
588 zoom-ins. Upper picture of zoom-ins shows epidermis on the top and dermis below. Lower
589 picture in zoom-ins shows hair follicle. H&E: Hematoxylin and eosin stain. gD: Staining against
590 HSV-1 glycoprotein D.
591
592 **Figure 2: Bulk RNA-seq of HSV-1 infected SkOs. A:** Barplot showing numbers of
593 differentially expressed host genes at 2, 4, 6, and 8dpi versus uninfected SkOs. **B:** GO analysis
594 (WebGestalt) was performed using significantly (padj. ≤0.05) up- or downregulated genes
595 (log2FC ≥1/≤-1) from RNA-seq analysis of SkOs infected with HSV-1 at 4, 6 and 8dpi
596 compared to uninfected SkOs. Shown are the top 5 significantly enriched GO-Terms (FDR
597 ≤0.01, sorted by enrichment ratio) in the up- and downregulated genes. At 2dpi no GO-terms
598 were significantly enriched. At 4dpi only 2 GO-terms were associated with the downregulated
599 genes. At 6dpi no GO-terms were significantly enriched in the upregulated genes. **C:**
600 Percentage of total reads mapping to HSV-1 in uninfected and 2, 4, 6, 8dpi. Each bar shows
601 one replicate.
602
603 **Figure 3: Spatial transcriptomics analysis of HSV-1 infected SkOs. A:** Representative
604 regions from an uninfected SkO (left) and a SkO at 3dpi (right), with cells colored by annotated
605 cell type. **B, C:** The same organoid regions as in A, colored by expression levels of the
606 indicated genes. **D:** Relative abundances of major cell types across the indicated timepoints.
607 Thin lines denote standard deviations calculated across three organoids per time point. Cell
608 type color coding is consistent with panel A.
609
610 **Figure 4: Susceptibility to viral infection varies widely between cell types. A:** Upper part:
611 percent of cells with at least 2 HSV-1 transcript counts for selected cell types. Indicated are
612 individual values from the three organoids per timepoint, and standard deviations. * p-value <
613 0.05 ** p-value < 0.01 (Student's t-test). Lower part: distribution of log10-transformed viral
614 loads (percent viral transcripts). The middle line in the boxplot displays the median, the box

615 indicates the first and third quartile, whiskers the 1.5 interquartile range (IQR). Outliers beyond
616 are marked by single dots. *** p-value < 0.001 (Wilcoxon rank sum test). **B:** Cells with at least
617 2 viral counts were ordered according to viral load and binned with 20 cells per bin. Shown are
618 the percentages of the two indicated viral transcripts within the bin for papillary fibroblasts type
619 1 (top) and stratum basale keratinocytes (bottom). **C:** Sections from WMI staining of HSV-1
620 infected SkOs harvested at the indicated dpi and stained for HSV-1 proteins ICP8 and gC.
621 Scale bars: 50µm. **D:** HSV-1 UL54 expression around HFs. Shown is a region from a SkO at
622 4dpi. Upper part: cells colored by cell type, with hair follicle cell types labeled. Lower part: cells
623 colored by normalized HSV-1 UL54 expression. Surrounded with orange are dermal sheaths
624 cells in proximity to highly infected papillary fibroblasts. **E:** Box plot of HSV-1 load (percent viral
625 transcripts) in HFs cells. Dermal sheath layer: Dermal sheath cells next to highly infected cells
626 (surrounded with orange in D). Outside/ inside: other cells within 50µm distance from dermal
627 sheath layer outside/ inside of HFs. **F:** Transmission electron microscopy (TEM) of HFs from
628 HSV-1 infected SkOs at 3dpi and 4dpi. Left images show overviews with colored layers of HFs.
629 pFib: papillary fibroblasts; DS: dermal sheath; GM: glassy membrane; Mtx: matrix; IRS: inner
630 root sheath; DP: dermal papilla; Ex: extracellular space; N: nucleus; C: cytoplasm. Boxes with
631 white and yellow lines, respectively indicate areas of zoom-ins. Red arrows indicate viral
632 particles. A and C capsids are indicated in a zoom-in on a nucleus of a matrix cell at 3dpi.
633
634 **Figure 5: IER3 is induced at the HSV-1 infection front in SkOs. A:** Papillary fibroblast types
635 1 and 2 with at least two viral RNA counts were clustered based on viral gene expression and
636 infection-induced host gene dysregulation, resulting in seven distinct clusters. Left: Two-
637 dimensional projection of cells colored by cluster membership. Right: Boxplot showing the
638 percentage viral transcripts in the cells of each cluster. **B:** Region of an infected organoid at
639 3dpi shown in Figure 3. Papillary fibroblasts are colored by cluster membership as in A, or in
640 light pink if containing less than two viral RNA counts (papillary fibroblasts without virus). Other
641 cell types, including “undefined” cells which includes highly infected papillary fibroblasts are in
642 light grey. **C:** Shown are transcript densities in papillary fibroblasts for genes as indicated in

643 spatial bins. Red colors indicate that both transcripts are present. VIM: Vimentin, general
644 marker for fibroblasts. **D:** Sections from WMI of uninfected and HSV-1 infected SkOs at 2dpi
645 and 3dpi stained for ICP8, IER3 and E-cadherin (marker for epidermis). Arrows indicate
646 potential site of viral infection that is shown in higher magnification below. Scale bars: 50µm.
647
648 **Figure 6: The transcription factor IRF3 is induced in keratinocytes. A:** Expression values
649 of the indicated genes in a subset of cell types. For uninfected and 2dpi SkOs, all cells were
650 combined for the analysis. For 3dpi and 4dpi, cells are split up in those with no or only 1 viral
651 count (-), and those with viral load below (+) and above (++) the median. The median viral load
652 was calculated only within cells with more than 1 count. Dot sizes represent the fraction of cells
653 having at least one count of the specified gene, the color the average expression. Black circles
654 around the dots indicate significant differential expression in a pseudobulk comparison vs. all
655 cells in uninfected cells (padj <0.05). **B:** Sections from WMI of uninfected and HSV-1 infected
656 SkOs at 3dpi and 4dpi stained for ICP8, IRF3 and E-cadherin (marker for epidermis). Scale
657 bars: 50µm.
658
659 **Figure 7:** TNF induction leads to proximal expression of target genes. **A:** Expression values
660 of the indicated genes in a subset of cell types. For uninfected and 2dpi SkOs, all cells were
661 combined for the analysis. For 3dpi and 4dpi, cells are split up in those with no or only 1 viral
662 count (-), and those with viral load below (+) and above (++) the median. The median viral load
663 was calculated only within cells with more than 1 count. Dot sizes represent the fraction of cells
664 having at least one count of the specified gene, the color the average expression. Black circles
665 around the dots indicate significant differential expression in a pseudobulk comparison vs. all
666 cells in uninfected cells (padj <0.05). **B:** Cells with at least 2 viral counts were ordered along
667 viral load and binned with 20 cells per bin. Shown are the percentages of TNF, TNFSF9 and
668 HSV-1 UL54 within the bin for papillary fibroblasts type 2 (top) and stratum basale
669 keratinocytes (bottom). **C:** Shown are two regions of a 4dpi organoid, with cells colored by cell
670 type or expression levels of the indicated genes. The cells encircled in red in the CXCL2

671 expression panel at 3dpi are expressing TNF. **D:** Differential expression of TNF target genes
672 in papillary fibroblasts proximal vs. distal to TNF expressing cell groups.
673
674 **Supplementary Figure 1: A:** Brightfield images of SkOs from day -2 (d-2) of differentiation to
675 126 days (d126). White scale bars represent 200µm, black scale bars 500µm. **B:** Maximum
676 intensity projections from Z-stacks of overview images from WMI staining of SkOs at 120 days
677 of differentiation. Scale bars 500µm. **C:** Zoom-ins of WMI staining. Scale bars 50µm. **D:** IHC
678 staining of SkOs at 120 days of differentiation. Boxes in overview images indicate areas of
679 higher magnification shown at the right. Scale bars represent 500µm in overview images and
680 50µm in zoom-ins. H&E: hematoxylin and eosin stain. Hoechst: nuclear stain. Ki67:
681 proliferating cells. KRT15: basal layer of epidermis, outer root sheath, medulla. KRT17:
682 epidermis, outer root sheath of HFs. KRT20: Merkel cells. KRT71: inner root sheath of HFs.
683 LHX2: bulge region, hair germs, hair pegs, hair placodes. NEFH: sensory neurons, large soma
684 neurons. PDGFRα: dermal fibroblasts, dermal papilla. S100β: Schwann cells, satellite glial
685 cells, adipocytes, melanocytes. SCD1: adipocytes, sebaceous glands. SOX2: dermal
686 condensates, dermal papilla, melanocytes, Merkel cells. TUBB3: neuronal cells, Schwann
687 cells.
688
689 **Supplementary Figure 2: A:** IHC staining against GFP of 120 days old SkOs infected with
690 HSV-1 expressing GFP from CMV-IE promoter. Boxes in overview images indicate areas of
691 higher magnification shown below. Scale bars 500µm in overview images and 20µm in zoom-
692 ins. Upper picture of zoom-ins shows epidermis on the top and dermis below. Lower picture in
693 zoom-ins shows hair follicle. **B:** Heatmap of bulk RNA-seq of HSV-1 infected SkOs showing
694 deregulated genes of HSV-1 infected SkOs at 2, 4, 6, and 8dpi vs uninfected SkOs in the
695 individual replicates. **C:** Volcano plots of bulk RNA-seq showing all differentially expressed
696 host genes at 2, 4, 6, and 8dpi vs uninfected SkOs.
697

698 **Supplementary Figure 3:** Spatial transcriptomics of HSV-1 infected SkOs. Per timepoint
699 (uninfected, 2dpi, 3dpi, 4dpi) 3 SkOs were measured. **A:** Overview of all SkOs analyzed by
700 spatial transcriptomics with cells colored by cell types. **B:** Cells as in A, colored by normalized
701 expression of HSV-1 UL54 RNA. **C:** Number of cells per organoid replicate. **D:** Violin plot
702 depicting distribution of detected genes and RNA counts for the major cell types.
703
704 **Supplementary Figure 4**. **A:** Papillary fibroblasts type 1 cells were binned according to their
705 distance from the organoid boundary (µm) in 10 bins of equal size. Other cell types as indicated
706 were sorted into the bins with the same distance range as the respective papillary fibroblasts
707 type 1 bin. By that, the distance distribution per bin is the same for all cell types (top panel),
708 but the fraction of cells per bin is equal only for papillary fibroblasts type 1 in all bins (bottom
709 panel), since the other cell types in general reside further inside the organoid. **B:** Top panel,
710 fraction of cells with at least two viral counts per distance bin. Bottom panel, viral load (percent
711 viral transcripts) in the different cell types per distance bins.
712
713 **Supplementary Figure 5: A:** Cells from SkOs at 4dpi were binned by cell type and by the
714 number of infectious cells (defined as >20% viral transcripts) in their neighborhood (within
715 50µm). Shown is the viral load (percent viral transcripts) per group as boxplots. The middle
716 line in the boxplot displays the median, the box indicates the first and third quartile, whiskers
717 the 1.5 interquartile range (IQR). Outliers beyond are marked by single dots. **B:** Shown is one
718 replicate of a HSV-1 infected SkO at 4dpi (bottom right of the 4dpi organoids in Supplementary
719 Figure 3A). Dermal sheath cells within 50µm of infectious cells (defined as >20% viral
720 transcripts) are labelled in dark blue. Cells of hair follicle cell types (dermal papilla, bulge
721 region, IRS, ORS, matrix, melanocytes) within 50µm of these dermal sheath cells are labelled
722 in medium pink. Other cell types (i.e., non-hair follicle cell types, thus outside of HFs, such as
723 papillary fibroblasts) are labelled in petrol. **C:** DAPI, cell surface protein and interior protein
724 staining on the Xenium slide. Surrounded with orange blue are dermal sheath cells as in Figure
725 4D.

726

727 **Supplementary Figure 6:** Scanning electron microscopy (SEM) of HFs from HSV-1 infected
728 SkOs at 3dpi and 4 dpi. **A:** Overviews showing the scanned areas. Black boxes indicate areas
729 scanned with higher resolution. White boxes with numbers indicate areas of zoom-ins shown
730 in B. pFib: papillary fibroblasts; DS: dermal sheath; GM: glassy membrane; ORS: outer root
731 sheath; parts of inner root sheath (IRS): Cp: companion layer, He: Henle‘s layer, Hu: Huxley‘s
732 layer, Ci: IRS cuticle; Mtx: matrix; DP: dermal papilla. Scale bar: 50µm. **B:** Zoom-ins on areas
733 indicated in part A. Red arrows indicate viral particles. Yellow boxes indicate areas of zoom-
734 ins showing extracellular viral particles and a nuclear replication compartment with A, B and C
735 capsids. RC: viral replication compartment; Ex: extracellular space, N: nucleus, C: cytoplasm.
736 Scale bar: 1µm; 200nm in zoom-ins.

737

738 **Supplementary Figure 7: A:** Two-dimensional projection of papillary fibroblasts as in Figure
739 5A, with cells colored by expression levels of the indicated host genome transcripts. **B:**
740 Papillary fibroblasts were categorized in “infection front” (cluster 1 in Fig. 5AB), “uninfected
741 next to infection front”, “infected next to infection front”, “later in infection” and “no virus” (i.e.,
742 without viral RNA and further away from the infection front). Top: two-dimensional projection
743 as in A, bottom: the same region as in Figure 5B, both with cells colored by these categories.
744 **C:** Differential gene expression in papillary fibroblasts in the cell categories shown in B at 3dpi
745 vs uninfected. Shown are the genes with padj < 0.05 in at least one category. **D:** Fold changes
746 in the bulk RNA-seq data at the indicated timepoints vs. uninfected organoids for IER3 and
747 selected induced host genes. Significantly upregulated genes have padj <0.05.

748

749

750 **Supplementary Figure 8: A:** Expression values of the indicated genes in a subset of cell
751 types. For uninfected and 2dpi SkOs, all cells were combined for the analysis. For 3dpi and
752 4dpi, cells are split up in those with no or only 1 viral count (-), and those with viral load below
753 (+) and above (++) the median. The median viral load was calculated only within cells with

754 more than 1 count. Dot sizes represent the fraction of cells having at least one count of the
755 specified gene, the color the average expression. Black circles around the dots indicate
756 significant differential expression in a pseudobulk comparison vs. all cells in uninfected cells
757 (padj <0.05). **B:** Fold changes in the bulk RNA-seq data at the indicated timepoints vs.
758 uninfected organoids for IRF3, TNF and TNFSF9. Significantly upregulated genes have padj
759 <0.05. **C:** Shown is one replicate of a HSV-1 infected SkO at 4dpi (top left of the 4dpi organoids
760 in Supplementary Figure 3A and Figure 7C). Cells are colored by TNF expressing cells,
761 proximal and distal cells as indicated.

762

763

764

765 ## References

766 1 James, C. *et al.* Herpes simplex virus: global infection prevalence and incidence
767 estimates, 2016. *Bull World Health Organ* **98**, 315-329 (2020).
768 https://doi.org:10.2471/BLT.19.237149
769 2 Zhu, S. & Viejo-Borbolla, A. Pathogenesis and virulence of herpes simplex virus.
770 *Virulence* **12**, 2670-2702 (2021). https://doi.org:10.1080/21505594.2021.1982373
771 3 Verzosa, A. L. *et al.* Herpes Simplex Virus 1 Infection of Neuronal and Non-Neuronal
772 Cells Elicits Specific Innate Immune Responses and Immune Evasion Mechanisms.
773 *Front Immunol* **12**, 644664 (2021). https://doi.org:10.3389/fimmu.2021.644664
774 4 Cunningham, A. L. *et al.* The cycle of human herpes simplex virus infection: virus
775 transport and immune control. *J Infect Dis* **194 Suppl 1**, S11-18 (2006).
776 https://doi.org:10.1086/505359
777 5 van Lint, A. *et al.* Herpes simplex virus-specific CD8+ T cells can clear established lytic
778 infections from skin and nerves and can partially limit the early spread of virus after
779 cutaneous inoculation. *J Immunol* **172**, 392-397 (2004).
780 https://doi.org:10.4049/jimmunol.172.1.392
781 6 Kollias, C. M., Huneke, R. B., Wigdahl, B. & Jennings, S. R. Animal models of herpes
782 simplex virus immunity and pathogenesis. *J Neurovirol* **21**, 8-23 (2015).
783 https://doi.org:10.1007/s13365-014-0302-2
784 7 Silva, J. R. *et al.* Neuroimmune-Glia Interactions in the Sensory Ganglia Account for
785 the Development of Acute Herpetic Neuralgia. *J Neurosci* **37**, 6408-6422 (2017).
786 https://doi.org:10.1523/JNEUROSCI.2233-16.2017
787 8 Wirtz, L., De La Cruz, N. C., Mockel, M. & Knebel-Morsdorf, D. Susceptibility of Human
788 and Murine Dermal Fibroblasts to Herpes Simplex Virus 1 in the Absence and Presence
789 of Extracellular Matrix. *J Virol* **96**, e0206821 (2022). https://doi.org:10.1128/JVI.02068-
790 21
791 9 Rahn, E. *et al.* Invasion of Herpes Simplex Virus Type 1 into Murine Epidermis: An Ex
792 Vivo Infection Study. *J Invest Dermatol* **135**, 3009-3016 (2015).
793 https://doi.org:10.1038/jid.2015.290

10 Wirtz, L., Mockel, M. & Knebel-Morsdorf, D. Invasion of Herpes Simplex Virus 1 into Murine Dermis: Role of Nectin-1 and Herpesvirus Entry Mediator as Cellular Receptors during Aging. *J Virol* **94** (2020). https://doi.org:10.1128/JVI.02046-19

11 De La Cruz, N. C. *et al.* Ex Vivo Infection of Human Skin with Herpes Simplex Virus 1 Reveals Mechanical Wounds as Insufficient Entry Portals via the Skin Surface. *J Virol* **95**, e0133821 (2021). https://doi.org:10.1128/JVI.01338-21

12 Tajpara, P. *et al.* A Preclinical Model for Studying Herpes Simplex Virus Infection. *J Invest Dermatol* **139**, 673-682 (2019). https://doi.org:10.1016/j.jid.2018.08.034

13 Sun, S., Jin, L., Zheng, Y. & Zhu, J. Modeling human HSV infection via a vascularized immune-competent skin-on-chip platform. *Nat Commun* **13**, 5481 (2022). https://doi.org:10.1038/s41467-022-33114-1

14 Andrei, G. *et al.* Organotypic epithelial raft cultures as a model for evaluating compounds against alphaherpesviruses. *Antimicrob Agents Chemother* **49**, 4671-4680 (2005). https://doi.org:10.1128/AAC.49.11.4671-4680.2005

15 Chu, J. T. S. & Lamers, M. M. Organoids in virology. *npj Viruses* **2**, 5 (2024). https://doi.org:10.1038/s44298-024-00017-5

16 Su, X. *et al.* Human Brain Organoids as an In Vitro Model System of Viral Infectious Diseases. *Front Immunol* **12**, 792316 (2021). https://doi.org:10.3389/fimmu.2021.792316

17 Shen, Q., Zhou, Y. H. & Zhou, Y. Q. A prospects tool in virus research: Analyzing the applications of organoids in virus studies. *Acta Trop* **254**, 107182 (2024). https://doi.org:10.1016/j.actatropica.2024.107182

18 Lee, J. *et al.* Hair-bearing human skin generated entirely from pluripotent stem cells. *Nature* **582**, 399-404 (2020). https://doi.org:10.1038/s41586-020-2352-3

19 Lee, J. *et al.* Generation and characterization of hair-bearing skin organoids from human pluripotent stem cells. *Nat Protoc* **17**, 1266-1305 (2022). https://doi.org:10.1038/s41596-022-00681-y

20 Hennig, T., Djakovic, L., Dolken, L. & Whisnant, A. W. A Review of the Multipronged Attack of Herpes Simplex Virus 1 on the Host Transcriptional Machinery. *Viruses* **13** (2021). https://doi.org:10.3390/v13091836

21 Gopee, N. H. *et al.* A prenatal skin atlas reveals immune regulation of human skin morphogenesis. *Nature* **635**, 679-689 (2024). https://doi.org:10.1038/s41586-024-08002-x

22 Trus, B. L. *et al.* Allosteric signaling and a nuclear exit strategy: binding of UL25/UL17 heterodimers to DNA-Filled HSV-1 capsids. *Mol Cell* **26**, 479-489 (2007). https://doi.org:10.1016/j.molcel.2007.04.010

23 Rutkowski, A. J. *et al.* Widespread disruption of host transcription termination in HSV-1 infection. *Nat Commun* **6**, 7126 (2015). https://doi.org:10.1038/ncomms8126

24 Wyler, E. *et al.* Widespread activation of antisense transcription of the host genome during herpes simplex virus 1 infection. *Genome Biol* **18**, 209 (2017). https://doi.org:10.1186/s13059-017-1329-5

25 Full, F. *et al.* Centrosomal protein TRIM43 restricts herpesvirus infection by regulating nuclear lamina integrity. *Nat Microbiol* **4**, 164-176 (2019). https://doi.org:10.1038/s41564-018-0285-5

26 Wyler, E. *et al.* Single-cell RNA-sequencing of herpes simplex virus 1-infected cells connects NRF2 activation to an antiviral program. *Nat Commun* **10**, 4878 (2019). https://doi.org:10.1038/s41467-019-12894-z

27 Full, F. *et al.* Herpesviruses mimic zygotic genome activation to promote viral replication. *Res Sq* (2023). https://doi.org:10.21203/rs.3.rs-3125635/v1

28 Neugebauer, E. *et al.* Herpesviruses mimic zygotic genome activation to promote viral replication. *Nat Commun* **16**, 710 (2025). https://doi.org:10.1038/s41467-025-55928-5

29 Uhlitz, F. *et al.* An immediate-late gene expression module decodes ERK signal duration. *Mol Syst Biol* **13**, 928 (2017). https://doi.org:10.15252/msb.20177554

30 Hsu, W. L., Saffran, H. A. & Smiley, J. R. Herpes simplex virus infection stabilizes cellular IEX-1 mRNA. *J Virol* **79**, 4090-4098 (2005). https://doi.org:10.1128/JVI.79.7.4090-4098.2005

31 Taddeo, B., Esclatine, A., Zhang, W. & Roizman, B. The stress-inducible immediate-early responsive gene IEX-1 is activated in cells infected with herpes simplex virus 1, but several viral mechanisms, including 3' degradation of its RNA, preclude expression of the gene. *J Virol* **77**, 6178-6187 (2003). https://doi.org:10.1128/jvi.77.11.6178-6187.2003

32 Corcoran, J. A., Hsu, W. L. & Smiley, J. R. Herpes simplex virus ICP27 is required for virus-induced stabilization of the ARE-containing IEX-1 mRNA encoded by the human IER3 gene. *J Virol* **80**, 9720-9729 (2006). https://doi.org:10.1128/JVI.01216-06

33 Haller, O. & Kochs, G. Mx genes: host determinants controlling influenza virus infection and trans-species transmission. *Hum Genet* **139**, 695-705 (2020). https://doi.org:10.1007/s00439-019-02092-8

34 Chopra, S. *et al.* Identification and characterization of collagen XXIII alpha 1 as a novel risk factor for eczema herpeticum. *medRxiv*, 2024.2007.2013.24310236 (2024). https://doi.org:10.1101/2024.07.13.24310236

35 Jones, K. *et al.* SOX4 and RELA Function as Transcriptional Partners to Regulate the Expression of TNF- Responsive Genes in Fibroblast-Like Synoviocytes. *Front Immunol* **13**, 789349 (2022). https://doi.org:10.3389/fimmu.2022.789349

36 Bai, L., Xu, J., Zeng, L., Zhang, L. & Zhou, F. A review of HSV pathogenesis, vaccine development, and advanced applications. *Mol Biomed* **5**, 35 (2024). https://doi.org:10.1186/s43556-024-00199-7

37 Gopinath, D., Koe, K. H., Maharajan, M. K. & Panda, S. A Comprehensive Overview of Epidemiology, Pathogenesis and the Management of Herpes Labialis. *Viruses* **15** (2023). https://doi.org:10.3390/v15010225

38 Rana, H., Truong, N. R., Sirimanne, D. R. & Cunningham, A. L. Breaching the Barrier: Investigating Initial Herpes Simplex Viral Infection and Spread in Human Skin and Mucosa. *Viruses* **16** (2024). https://doi.org:10.3390/v16111790

39 Richardo, T. *et al.* Herpes simplex virus assembly and spread in murine skin after infection from the outside. *J Virol* **99**, e0163824 (2025). https://doi.org:10.1128/jvi.01638-24

40 Petermann, P. *et al.* Entry mechanisms of herpes simplex virus 1 into murine epidermis: involvement of nectin-1 and herpesvirus entry mediator as cellular receptors. *J Virol* **89**, 262-274 (2015). https://doi.org:10.1128/JVI.02917-14

41 Barreau, C., Paillard, L. & Osborne, H. B. AU-rich elements and associated factors: are there unifying principles? *Nucleic Acids Res* **33**, 7138-7150 (2005). https://doi.org:10.1093/nar/gki1012

42 Dean, J. L., Sully, G., Clark, A. R. & Saklatvala, J. The involvement of AU-rich element-binding proteins in p38 mitogen-activated protein kinase pathway-mediated mRNA stabilisation. *Cell Signal* **16**, 1113-1121 (2004). https://doi.org:10.1016/j.cellsig.2004.04.006

43 Rybak-Wolf, A. *et al.* Modelling viral encephalitis caused by herpes simplex virus 1 infection in cerebral organoids. *Nat Microbiol* **8**, 1252-1266 (2023). https://doi.org:10.1038/s41564-023-01405-y

44 Oyler-Yaniv, J., Oyler-Yaniv, A., Maltz, E. & Wollman, R. TNF controls a speed-accuracy tradeoff in the cell death decision to restrict viral spread. *Nat Commun* **12**, 2992 (2021). https://doi.org:10.1038/s41467-021-23195-9

45 Hafezi, W. *et al.* Entry of herpes simplex virus type 1 (HSV-1) into the distal axons of trigeminal neurons favors the onset of nonproductive, silent infection. *PLoS Pathog* **8**, e1002679 (2012). https://doi.org:10.1371/journal.ppat.1002679

46 Ewels, P. A. *et al.* The nf-core framework for community-curated bioinformatics pipelines. *Nat Biotechnol* **38**, 276-278 (2020). https://doi.org:10.1038/s41587-020-0439-x

47 Di Tommaso, P. *et al.* Nextflow enables reproducible computational workflows. *Nat Biotechnol* **35**, 316-319 (2017). https://doi.org:10.1038/nbt.3820

48 Dobin, A. *et al.* STAR: ultrafast universal RNA-seq aligner. *Bioinformatics* **29**, 15-21 (2013). https://doi.org:10.1093/bioinformatics/bts635

49 Patro, R., Duggal, G., Love, M. I., Irizarry, R. A. & Kingsford, C. Salmon provides fast and bias-aware quantification of transcript expression. *Nat Methods* **14**, 417-419 (2017). https://doi.org:10.1038/nmeth.4197

50 Soneson, C., Love, M. & Robinson, M. Differential analyses for RNA-seq: transcript-level estimates improve gene-level inferences [version 1; peer review: 2 approved]. *F1000Research* **4** (2015). https://doi.org:10.12688/f1000research.7563.1

51 Love, M. I., Huber, W. & Anders, S. Moderated estimation of fold change and dispersion for RNA-seq data with DESeq2. *Genome Biol* **15**, 550 (2014). https://doi.org:10.1186/s13059-014-0550-8

52 Elizarraras, J. M. *et al.* WebGestalt 2024: faster gene set analysis and new support for metabolomics and multi-omics. *Nucleic Acids Res* **52**, W415-W421 (2024). https://doi.org:10.1093/nar/gkae456

53 Manukyan, A. *et al.* VoltRon: A Spatial Omics Analysis Platform for Multi-Resolution and Multi-omics Integration using Image Registration. *bioRxiv*, 2023.2012.2015.571667 (2023). https://doi.org:10.1101/2023.12.15.571667

54 Wickham, H. *et al.* Welcome to the Tidyverse. *Journal of Open Source Software* **4**, 1686 (2019). https://doi.org:10.21105/joss.01686

55 Zhu, A., Ibrahim, J. G. & Love, M. I. Heavy-tailed prior distributions for sequence count data: removing the noise and preserving large differences. *Bioinformatics* **35**, 2084-2092 (2019). https://doi.org:10.1093/bioinformatics/bty895

56 Pebesma, E. Simple Features for R: Standardized Support for Spatial Vector Data. *The R Journal* **10**, 439-446 (2018). https://doi.org:10.32614/RJ-2018-009

57 Gombin, J., Vaidyanathan, R. & Agafonkin, V. concaveman: A Very Fast 2D Concave Hull Algorithm. (2020).

Figure 1

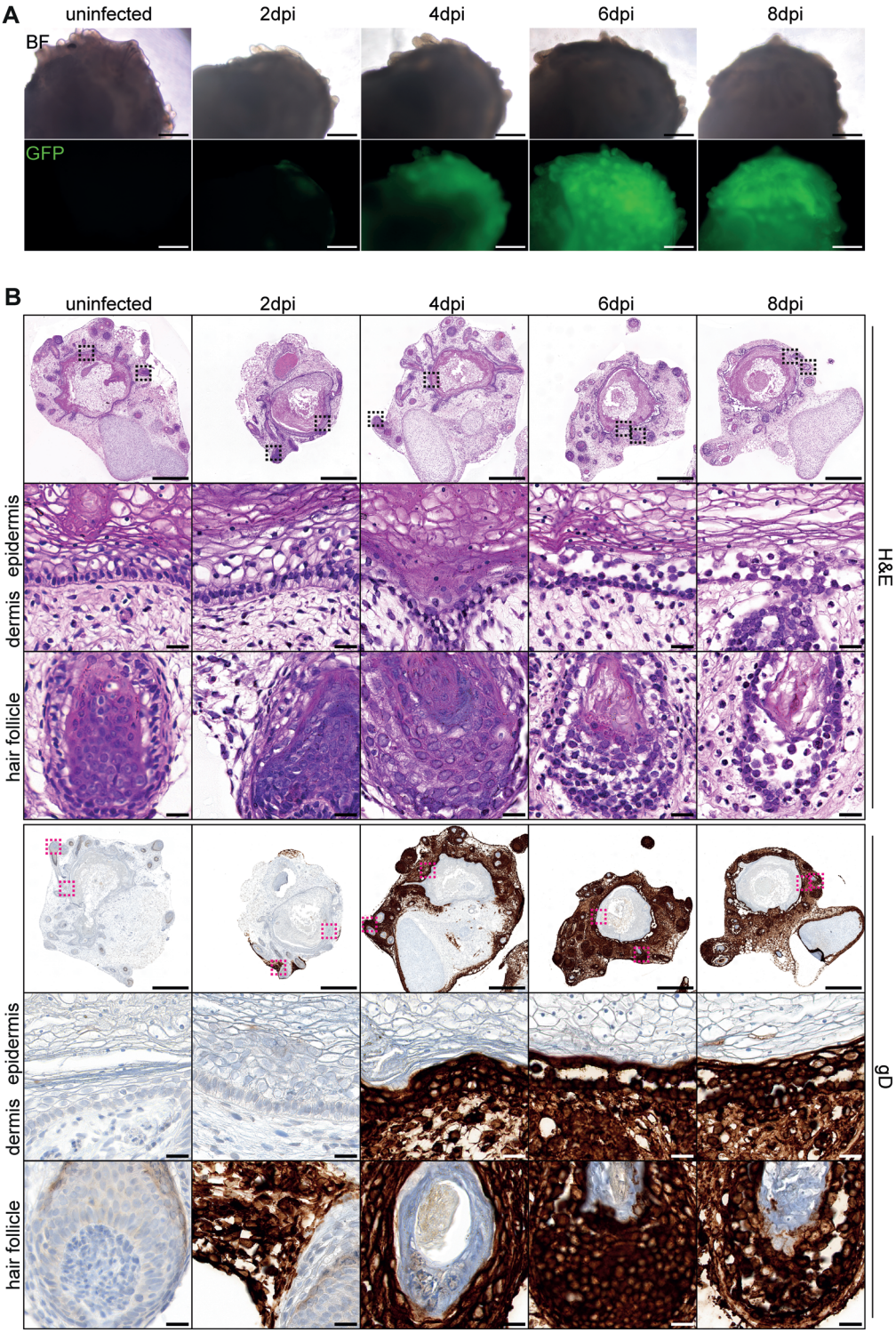

Figure 1: Infection of skin organoids with HSV-1 leads to cytopathic effects. A: Brightfield (BF) and fluorescence (GFP) images of skin organoids (SkOs) infected with HSV-1 (expressing GFP from a CMV-IE promoter) at 120 days of differentiation. Shown are uninfected and HSV-1 infected SkOs at 2, 4, 6, and 8 days post infection (dpi). Scale bars 500µm. **B:** IHC staining of SkOs infected with HSV-1 as shown in A. Boxes in overview images indicate areas of higher magnification shown below. Scale bars 500µm in overview images and 20µm in zoom-ins. Upper picture of zoom-ins shows epidermis on the top and dermis below. Lower picture in zoom-ins shows hair follicle. H&E: Hematoxylin and eosin stain. gD: Staining against HSV-1 glycoprotein D.

Figure 2

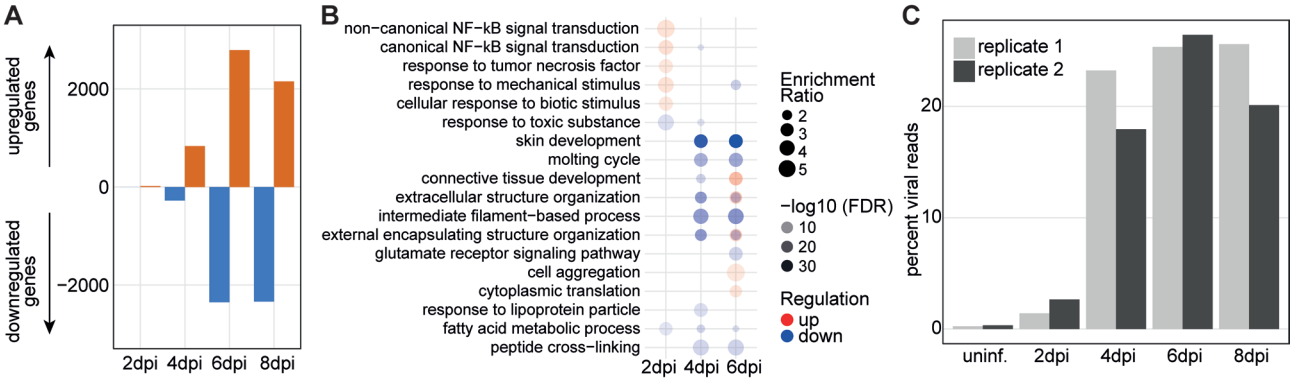

Figure 2: Bulk RNA-seq of HSV-1 infected SkOs. A: Barplot showing numbers of differentially expressed host genes at 2, 4, 6, and 8dpi versus uninfected SkOs. **B:** GO analysis (WebGestalt) was performed using significantly (padj. ≤0.05) up- or downregulated genes (log2FC ≥1/≤-1) from RNA-seq analysis of SkOs infected with HSV-1 at 4, 6 and 8dpi compared to uninfected SkOs. Shown are the top 5 significantly enriched GO-Terms (FDR ≤0.01, sorted by enrichment ratio) in the up- and downregulated genes. At 2dpi no GO-terms were significantly enriched. At 4dpi only 2 GO-terms were associated with the downregulated genes. At 6dpi no GO-terms were significantly enriched in the upregulated genes. **C:** Percentage of total reads mapping to HSV-1 in uninfected and 2, 4, 6, 8dpi. Each bar shows one replicate.

Figure 3

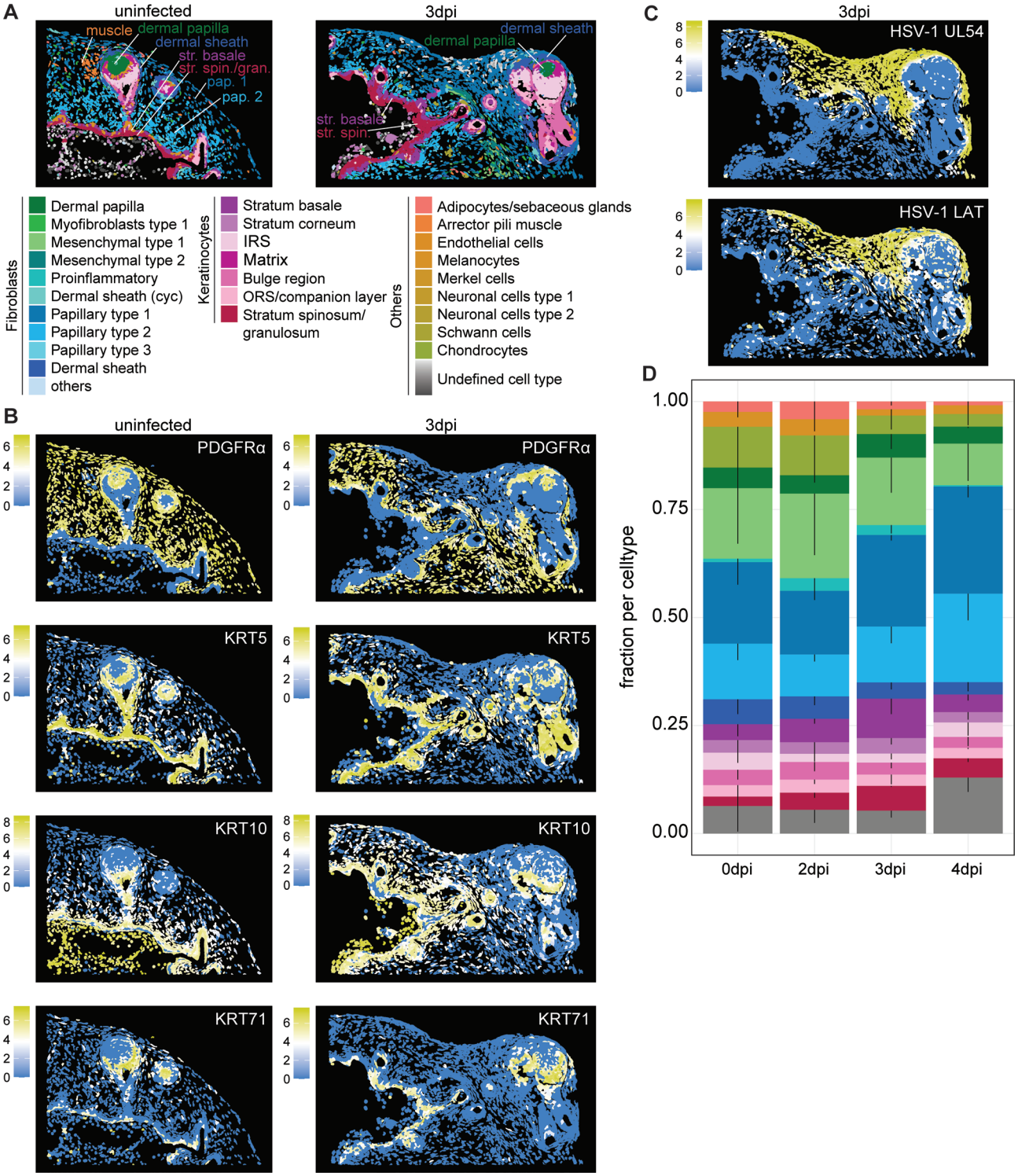

Figure 3: Spatial transcriptomics analysis of HSV-1 infected SkOs. A: Representative regions from an uninfected SkO (left) and a SkO at 3dpi (right), with cells colored by annotated cell type. **B, C:** The same organoid regions as in A, colored by expression levels of the indicated genes. **D:** Relative abundances of major cell types across the indicated timepoints. Thin lines denote standard deviations calculated across three organoids per time point. Cell type color coding is consistent with panel A.

Figure 4

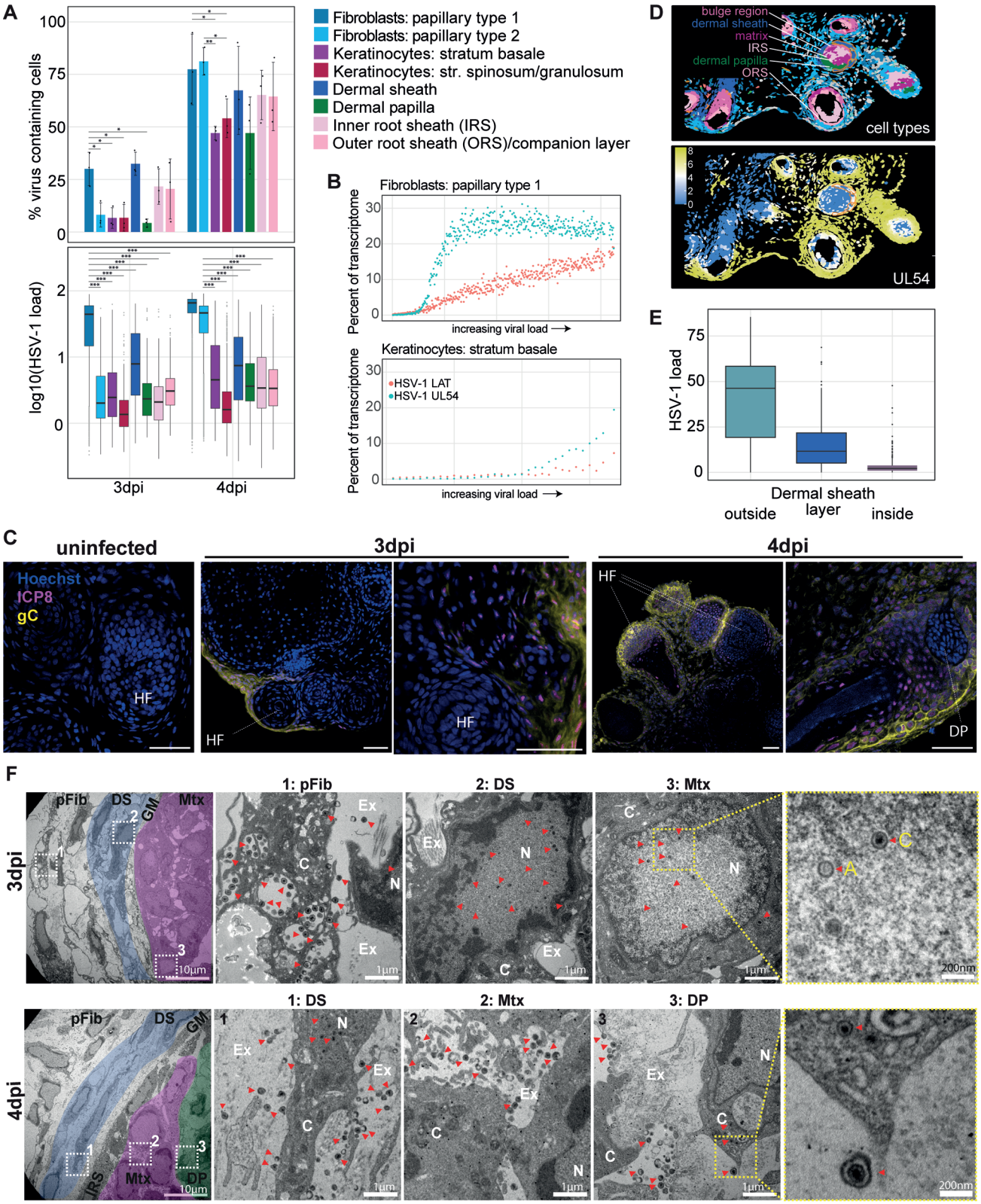

Figure 4: Susceptibility to viral infection varies widely between cell types. A: Upper part: percent of cells with at least 2 HSV-1 transcript counts for selected cell types. Indicated are individual values from the three organoids per timepoint, and standard deviations. * p-value < 0.05 ** p-value < 0.01 (Student's t-test). Lower part: distribution of log10-transformed viral loads (percent viral transcripts). The middle line in the boxplot displays the median, the box indicates the first and third quartile, whiskers the 1.5 interquartile range (IQR). Outliers beyond are marked by single dots. *** p-value < 0.001 (Wilcoxon rank sum test). **B:** Cells with at least 2 viral counts were ordered according to viral load and binned with 20 cells per bin. Shown are the percentages of the two indicated viral transcripts within the bin for papillary fibroblasts type 1 (top) and stratum basale keratinocytes (bottom). **C:** Sections from WMI staining of HSV-1 infected SkOs harvested at the indicated dpi and stained for HSV-1 proteins ICP8 and gC. Scale bars: 50µm. **D:** HSV-1 UL54 expression around HFs. Shown is a region from a SkO at 4dpi. Upper part: cells colored by cell type, with hair follicle cell types labeled. Lower part: cells colored by normalized HSV-1 UL54 expression. Surrounded with orange are dermal sheaths cells in proximity to highly infected papillary fibroblasts. **E:** Box plot of HSV-1 load (percent viral transcripts) in HFs cells. Dermal sheath layer: Dermal sheath cells next to highly infected cells (surrounded with orange in D). Outside/ inside: other cells within 50µm distance from dermal sheath layer outside/ inside of HFs. **F:** Transmission electron microscopy (TEM) of HFs from HSV-1 infected SkOs at 3dpi and 4dpi. Left images show overviews with colored layers of HFs. pFib: papillary fibroblasts; DS: dermal sheath; GM: glassy membrane; Mtx: matrix; IRS: inner root sheath; DP: dermal papilla; Ex: extracellular space; N: nucleus; C: cytoplasm. Boxes with white and yellow lines, respectively indicate areas of zoom-ins. Red arrows indicate viral particles. A and C capsids are indicated in a zoom-in on a nucleus of a matrix cell at 3dpi.

Figure 5

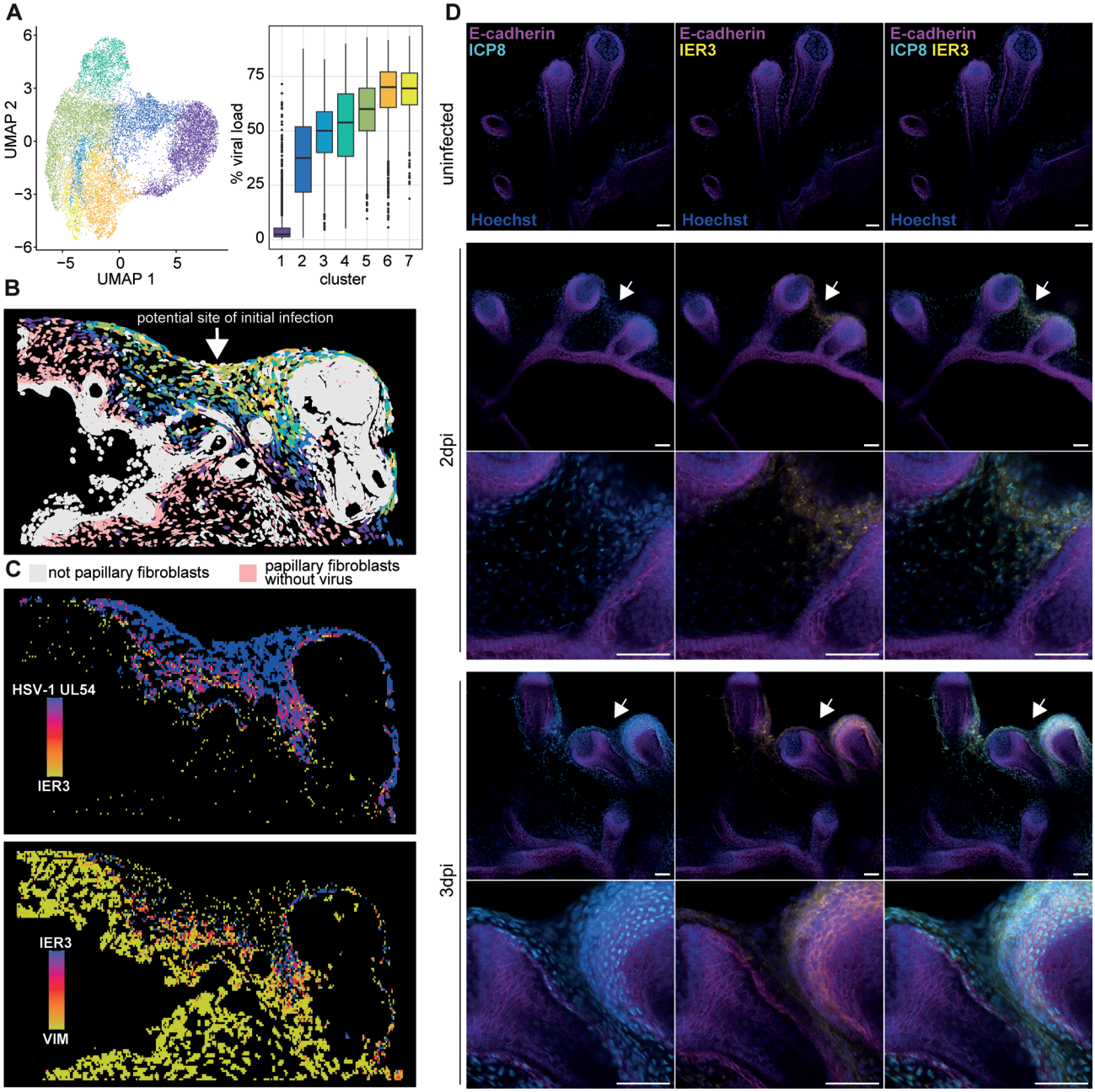

Figure 5: IER3 is induced at the HSV-1 infection front in SkOs. A: Papillary fibroblast types 1 and 2 with at least two viral RNA counts were clustered based on viral gene expression and infection-induced host gene dysregulation, resulting in seven distinct clusters. Left: Two-dimensional projection of cells colored by cluster membership. Right: Boxplot showing the percentage viral transcripts in the cells of each cluster. **B:** Region of an infected organoid at 3dpi shown in Figure 3. Papillary fibroblasts are colored by cluster membership as in A, or in light pink if containing less than two viral RNA counts (papillary fibroblasts without virus). Other cell types, including "undefined" cells which includes highly infected papillary fibroblasts are in light grey. **C:** Shown are transcript densities in papillary fibroblasts for genes as indicated in spatial bins. Red colors indicate that both transcripts are present. VIM: Vimentin, general marker for fibroblasts. **D:** Sections from WMI of uninfected and HSV-1 infected SkOs at 2dpi and 3dpi stained for ICP8, IER3 and E-cadherin (marker for epidermis). Arrows indicate potential site of viral infection that is shown in higher magnification below. Scale bars: 50µm.

Figure 6

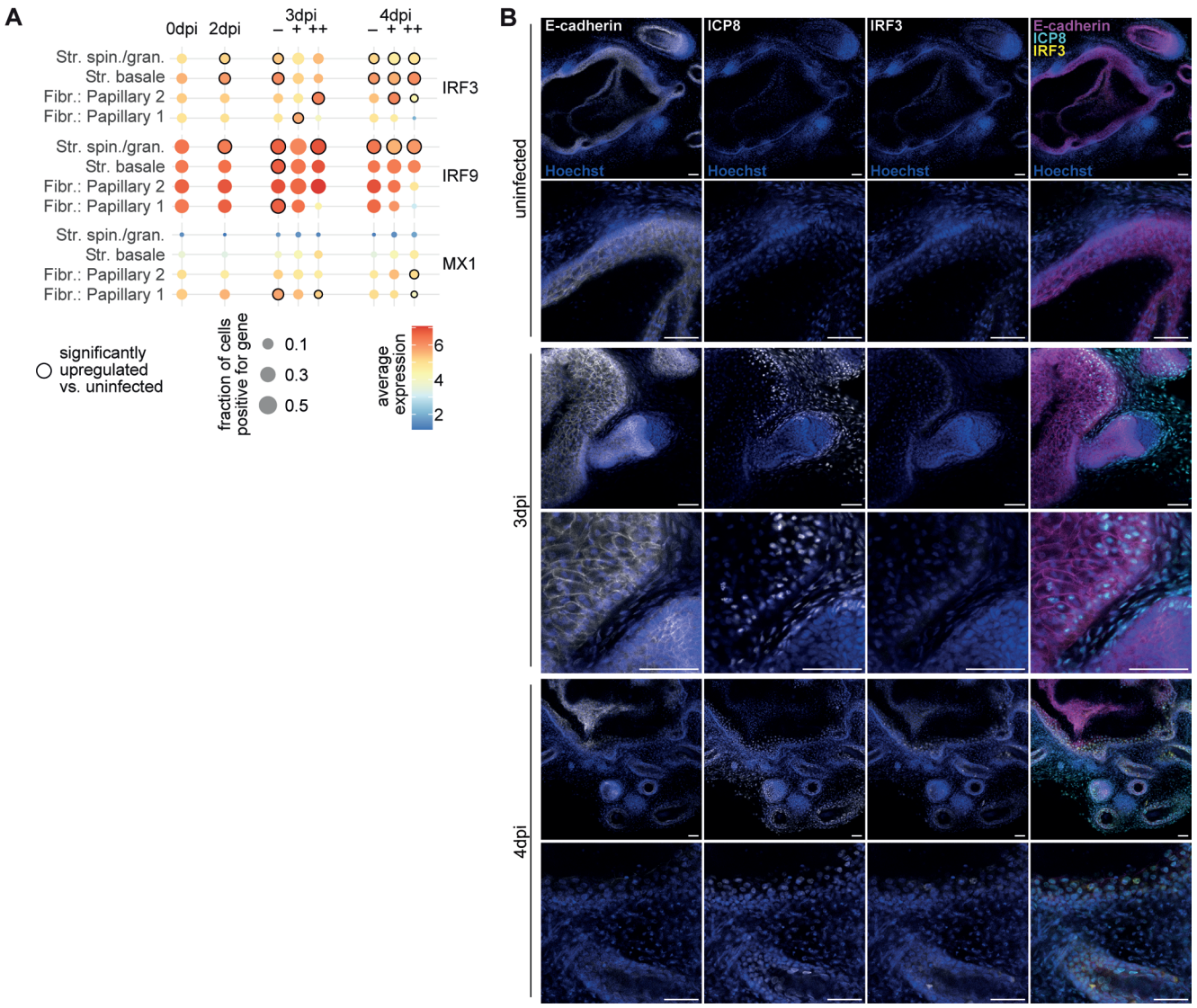

Figure 6: The transcription factor IRF3 is induced in keratinocytes. A: Expression values of the indicated genes in a subset of cell types. For uninfected and 2dpi SkOs, all cells were combined for the analysis. For 3dpi and 4dpi, cells are split up in those with no or only 1 viral count (-), and those with viral load below (+) and above (++) the median. The median viral load was calculated only within cells with more than 1 count. Dot sizes represent the fraction of cells having at least one count of the specified gene, the color the average expression. Black circles around the dots indicate significant differential expression in a pseudobulk comparison vs. all cells in uninfected cells (padj <0.05). **B:** Sections from WMI of uninfected and HSV-1 infected SkOs at 3dpi and 4dpi stained for ICP8, IRF3 and E-cadherin (marker for epidermis). Scale bars: 50µm.

Figure 7

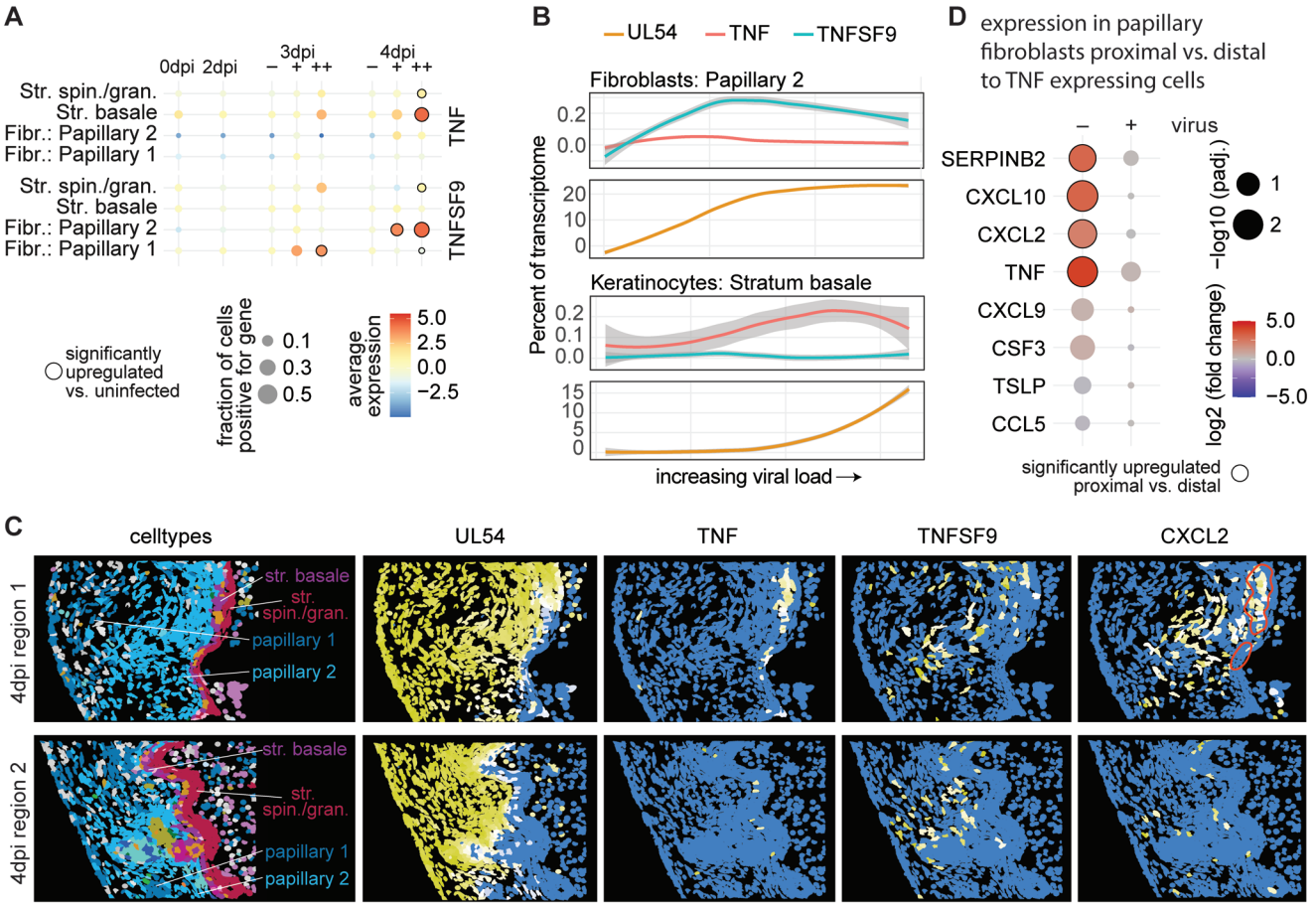

Figure 7: TNF induction leads to proximal expression of target genes. A: Expression values of the indicated genes in a subset of cell types. For uninfected and 2dpi SkOs, all cells were combined for the analysis. For 3dpi and 4dpi, cells are split up in those with no or only 1 viral count (-), and those with viral load below (+) and above (++) the median. The median viral load was calculated only within cells with more than 1 count. Dot sizes represent the fraction of cells having at least one count of the specified gene, the color the average expression. Black circles around the dots indicate significant differential expression in a pseudobulk comparison vs. all cells in uninfected cells (padj <0.05). **B:** Cells with at least 2 viral counts were ordered along viral load and binned with 20 cells per bin. Shown are the percentages of TNF, TNFSF9 and HSV-1 UL54 within the bin for papillary fibroblasts type 2 (top) and stratum basale keratinocytes (bottom). **C:** Shown are two regions of a 4dpi organoid, with cells colored by cell type or expression levels of the indicated genes. The cells encircled in red in the CXCL2 expression panel at 3dpi are expressing TNF. D: Differential expression of TNF target genes in papillary fibroblasts proximal vs. distal to TNF expressing cell groups.